Available on CMS information server **CMS NOTE 2006-130**

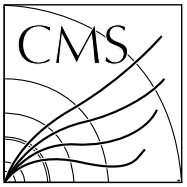

The Compact Muon Solenoid Experiment

CMS Note

Mailing address: CMS CERN, CH-1211 GENEVA 23, Switzerland

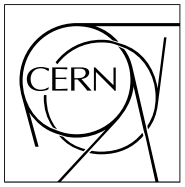

15 June 2006

NLO vs. LO: kinematical differences for signal and background in the $H \to ZZ^* \to 4\mu$ analysis

P. Bartalini[1], A. Drozdetskiy[1], A. Korytov[1], G. Mitselmakher[1], A. Sherstnev[2,3], H. Stenzel[4]

Abstract

In the note we present a comparison of Monte-Carlo kinematical distributions in the LO+PS and the NLO approximation for the single Higgs production with decay to four muons at the LHC and for its main irreducible background, the double Z/γ production process. The choice of the distributions is driven by the potential for discriminating signal vs. $t\bar{t}$, $Z/\gamma + b\bar{b}(c\bar{c})$, and double Z/γ backgrounds.

[1)] University of Florida, FL, USA

[2)] Moscow State University, Moscow, Russia

[3)] Cavendish Laboratory, University of Cambridge, UK

[4)] Ruprecht-Karls-Universitat Heidelberg, Heidelberg, Germany

[5)] Preprint CAVENDISH-HEP-06-19

1 Introduction

One of the most important tasks of the research program at the LHC is the investigation of the electroweak symmetry breaking phenomenon. In the Standard Model the Higgs mechanism is responsible for the effect and the most apparent evidence of the mechanism is to observe the direct Higgs boson production at the LHC. There are a number of different channels to search for a Higgs at the collider (see the corresponding section of the review [1]) and both collaborations on the general purpose detectors, CMS and ATLAS, have their own Higgs programs [2, 3].

The CMS detector has a very advanced and reliable muon detection system. One of the cleanest patterns of Higgs production at CMS will be in the "golden" channel, with four muons in the final state arising from the process ($pp \to H \to ZZ^* \to 4\mu$). This channel has the following backgrounds: the double Z/γ production (the main irreducible background), the $t\bar{t}$ production and the $Z/\gamma + b\bar{b}(c\bar{c})$ processes. In the second and third process the additional necessary muon pair appears from the c/b-quark semileptonic decays. The double Z/γ process should include Z-, γ-, and Z/γ interference contribution. Since this process gives the main contribution to the overall background, this note will particularly concentrate on its specific features.

Reliable experimental analyses should take into account all appropriate theoretical uncertainties. In the note we focus on the influence of the NLO QCD corrections to both signal and main background.

In general, these corrections are large for many processes of interest at the LHC energies. The NLO corrections for the Higgs production were calculated some years ago [4]. It was found that these corrections account for cross sections up to 2-3 times higher with respect to the process described at LO. Thanks to the recent refinement of Monte Carlo tools at NLO, like MC@NLO [5], it is now possible to study the examined process in further details, evaluating the impact of the NLO correction on the dynamics, and understanding to what extent they affect the kinematical selection criteria adopted in the $H \to ZZ^* \to 4\mu$ search.

NLO corrections to the double Z/γ production process were calculated in [6]. MC@NLO implements this process, however it does not include γ and Z/γ interference contributions and the Z-boson width. Since these effects are expected to be relevant, especially in the low Higgs mass range, NLO events for this process will be simulated adopting a special algorithm [7] (see section 5).

The ultimate goal of this note is to quantify the influence of the NLO corrections on the signal/background separation according to different $H \to ZZ^* \to 4\mu$ search scenarios.

In the next section we briefly document the event generation performed for this study. In section 3 we introduce all the different kinematical selections used in our analysis. The NLO dynamics of the Higgs production is considered in section 4. The double Z/γ^* production process is described in section 5. Influence of the NLO corrections on our analysis scenario is discussed in section 6. Conclusions are given in section 7.

2 Physics model

For the analysis described in this note we used several Monte-Carlo codes.

In order to prepare LO Monte-Carlo event samples we employed HERWIG [8] (Higgs pro-

duction) and MadGraph/MadEvent [9] (double Z/γ production). Strictly speaking HERWIG is not a LO generator, since it adds parton showering effects to the events, so we will call the approximation realized in the code (as also in PYTHIA) as a LO+PS approximation.

Higgs production at NLO is simulated with MC@NLO [5, 10], while a special procedure is adopted to simulate double Z/γ production at NLO. This procedure, which was employed for the first time in single t-quark production [7], is described in the note (see section 5) and relies on the combined usage of MadGraph/MadEvent, PYTHIA [11] and MCFM [12].

One of the most interesting features of MC@NLO is the possibility to produce fully exclusive events at NLO.

The events are generated with weights and then interfaced with HERWIG in order to take into account both exact NLO corrections and parton shower effects. We used the MC@NLO program to prepare samples of the Higgs production for the Higgs masses M_H= 150 GeV and 250 GeV.

The choice of HERWIG as a cross section estimator and event generator for Higgs production at LO is motivated by the intention to reduce to the minimum unwanted biases when comparing with NLO. Indeed this code is also used internally by MC@NLO (as explained above). HERWIG implements tree-level diagram calculations for the Higgs production process.

HDECAY [13] was used in order to get the NLO description for the Higgs width.

In order to generate events for the double Z/γ-boson production we need the full cross sections at NLO for different sets of cuts (signal separation scenarios are reported below). These numbers have been calculated using the MCFM code, taking into account the effects of Z/γ-interference and the Z-boson width.

MadGraph is an event generator at tree-level. It uses helicity amplitudes to calculate cross sections and to generate events (strictly speaking, it uses the HELAS package [14] to calculate the helicity amplitudes). PYTHIA is adopted to simulate the shower evolution starting from the parton level configuration provided by MadGraph.

The following set of physics parameters has been adopted in event generation:

- $\alpha = 1/127.9$
- $\sin\theta_W = 0.48076$;
- M_Z = 91.1876 GeV, Γ_Z = 2.495 GeV;
- M_W = 79.958 GeV, Γ_W = 2.12 GeV;
- (M_H,Γ_H) = (150 GeV, 16.98 MeV), (250 GeV, 4.046 GeV), (500 GeV, 67.88 GeV);
- M_t = 175.0 GeV, Γ_t is calculated by the codes;
- M_b = 4.85 GeV, M_c = 1.65 GeV;
- CTEQ5 Parton Density Functions (PDF) [15]: cteq5l (for all LO+PS calculations), cteq5m1 (for all NLO calculations);
- QCD scale: $Q^2_{QCD} = \hat{s}^{1)}$ (for all calculations).

3 Kinematical cuts used

For the study we have defined three different selection criteria: pre-selection cuts, selection cuts, and analysis cuts. The first set of cuts is applied to generate ideal events on the particle level. Selection cuts are applied on the events after detailed simulation and reconstruction in the CMS experiment which is performed with the official framework prepared by the collaboration. Analysis cuts are adopted at the analysis level, where the goal is to get rid of background processes keeping an "acceptable" signal efficiency. In principle these cuts should depend on the Higgs mass. However we don't restrict ourself to narrow $M_{inv}(4\mu)$ ranges.

Hereafter, we will use two objects, constructed from final muons in our analysis. The $Z1$-boson is defined as the virtual object made by the two opposite-sign muons whose invariant mass better approximates the nominal Z-boson mass. Instead, the $Z2$-boson is made out of the remnant muon pair. If an event has more then four muons, we choose the four highest-P_T muons to construct the objects. μ_1, ..., μ_4 are all muons in the event sorted according to P_T.

Pre-selection cuts:

- $M_{inv}(4\mu) < 1000$ GeV
- 3 GeV $< P_T(\mu)$, $|\eta(\mu)| < 2.4$
- 5 GeV $< M_{inv}(\mu^+\mu^-) < 1000$ GeV
- 5 GeV $< M_{inv}(Z1) < 150$ GeV, 5 GeV $< M_{inv}(Z2) < 150$ GeV

Selection cuts:

- $M_{inv}(4\mu) < 1000$ GeV
- 7 GeV $< P_T(\mu)$ for $|\eta(\mu)| < 1.1$ and 13 GeV $< P(\mu)$ for $1.1 < |\eta(\mu)| < 2.4$
- 12 GeV $< M_{inv}(\mu^+\mu^-) < 1000$ GeV
- 12 GeV $< M_{inv}(Z1) < 150$ GeV, 12 GeV $< M_{inv}(Z2) < 150$ GeV

Analysis cuts:

- 12 GeV $< M_{inv}(Z1) < 150$ GeV, 12 GeV $< M_{inv}(Z2) < 150$ GeV
- 12 GeV $< M_{inv}(\mu^+\mu^-) < 1000$ GeV
- 110 GeV $< M_{inv}(4\mu) < 700$ GeV (a broad $M_{inv}(4\mu)$ window)
- $|\eta(\mu)| < 2.4$
- 14 GeV $< P(\mu_1)$, 10 GeV $< P_T(\mu_2)$, 10 GeV $< P_T(\mu_3)$,7 GeV $< P_T(\mu_4)$
- Muon track isolation cut (not applied in the study)
- Narrow $M_{inv}(4\mu)$ window cut (depends on the Higgs mass value, also not applied here)

[1)] $\hat{s}$ is defi ned by a standard way: $\hat{s}=(p_1+p_2)^2$, where $p_{1,2}$ – 4-momenta of the initial partons.

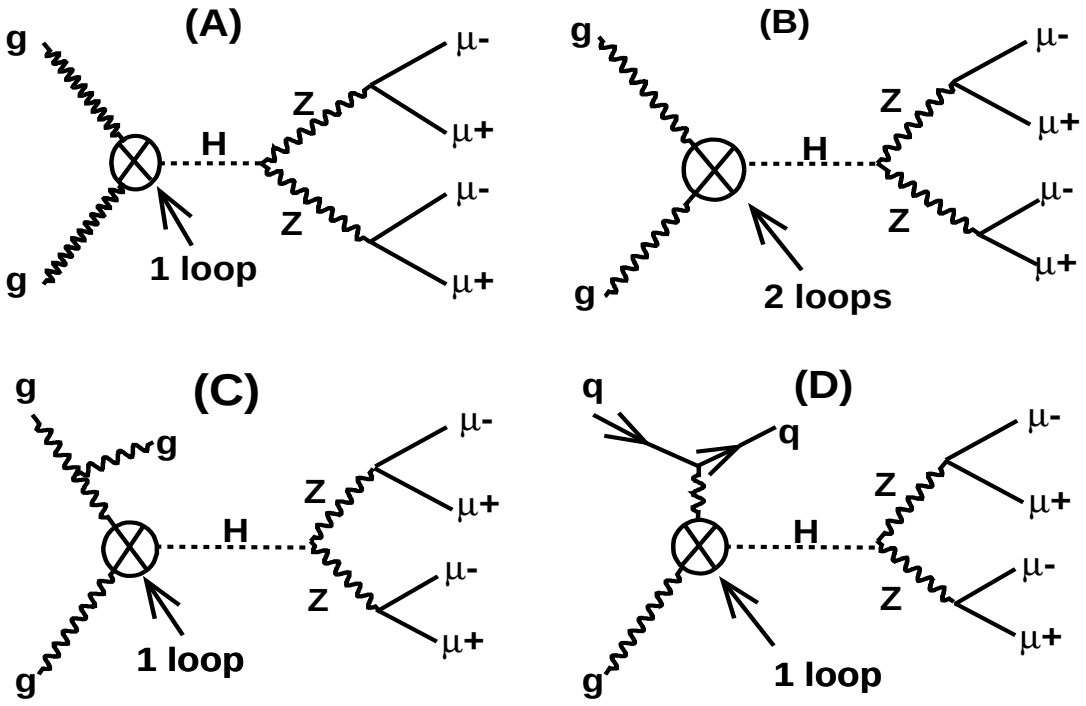

Figure 1: LO (A) and NLO (B,C,D) diagrams for the process $pp \to H \to ZZ^* \to 4\mu$.

4 The $pp \to H \to ZZ^* \to 4\mu$ process

The single Higgs production at LO occurs through triangle loops of massive quarks. In our study we investigate Higgs decay to two Z-bosons with subsequent decay to four muons. LO (A) and NLO (B,C,D) diagrams are illustrated in Fig. 1.

Since the Higgs mass is unknown so far, we considered two different values of the parameter in our analysis, M_H = 150 and 250 GeV. We also tried M_H = 500 GeV, however some HERWIG limitations showed up in this case, as the program turns out not to treat the case of large Higgs widths in an appropriate way.

We prepared 250000 events for each Higgs mass at LO+PS with no cuts. The full cross sections and the numbers of events for different sets of cuts can be found in Tabs. 1 and 2.

Although the full Higgs production cross section decreases with the Higgs mass, due to the large Z-boson mass, the branching ratio $Br(H \to ZZ)$ depends on M_H in a complicated way [16]. The most crucial limit is the threshold of double real Z-boson production ($M_H = 2M_Z$). Lower rates are expected for M_H = 150 GeV (Higgs production below the threshold) than in the case of M_H = 250 GeV (above the threshold), as you can see in the tables with cross sections.

4.1 Monte-Carlo simulation (M_H = 150 GeV)

Kinematical distributions for the Higgs production with mass M_H = 150 GeV are reported in Figs. 2–6.

P_T and pseudorapidity distributions for the four final muons sorted according to their P_T are

Table 1: Cross sections of the single Higgs production with decay to four muons at LO+PS and at NLO (M_H = 150 GeV), and the corresponding expected numbers of events for 30 fb^{-1} integrated luminosity. The last column presents K-factors: K=$\sigma_{NLO}/\sigma_{LO+PS}$.

Cuts	LO+PS		NLO		
	σ_{LO+PS}, fb	N_{events}	σ_{NLO}, fb	N_{events}	K-factor
no cuts	0.900	27.0	2.21	66.2	2.45
pre-selection cuts	0.533	16.0	1.31	39.3	2.46
selection cuts	0.470	14.1	1.16	34.8	2.47
Analysis cuts	0.447	13.4	1.10	33.0	2.46

Table 2: Cross sections of the single Higgs production with decay to four muons at LO+PS and at NLO (M_H = 250 GeV), and the corresponding expected numbers of events for 30 fb^{-1} integrated luminosity. The last column presents K-factors: K=$\sigma_{NLO}/\sigma_{LO+PS}$.

Cuts	LO+PS		NLO		
	σ_{LO}, fb	N_{events}	σ_{NLO}, fb	N_{events}	K-factor
no cuts	1.34	40.3	3.04	91.3	2.27
pre-selection cuts	0.897	26.9	2.03	60.9	2.26
selection cuts	0.880	26.4	2.00	59.9	2.26
Analysis cuts	0.870	26.1	1.97	59.1	2.26

shown in Figs. 2 and 3 respectively. All muons are slightly harder at NLO, in particular the highest P_T muon. No large differences between the pseudorapidity distributions at LO and NLO are expected.

Invariant mass and P_T distributions for the $Z1$- and $Z2$-boson are reported in Fig. 4. Both Z-bosons have larger P_T at the NLO, but the effect is rather small. The mass distributions do not show significant differences.

The most interesting distributions deal with the Higgs boson kinematics: invariant mass and transverse momentum P_T. These distributions are reported in Fig. 5. One can see a strong dependence of the K-factor on the Higgs P_T. There is a small shift of the Higgs mass peak due to a small inconsistency of the initial gluon kinematics in HERWIG. Calculations of the matrix element squared of the process use massless gluons. But event generation in HERWIG requires massive gluons due to features of the HERWIG QCD showering algorithm. It gives an additional shift $\approx m_g^2/m_H$ of the Higgs mass peak from a nominal mass [17]. This effect is tiny and becomes smaller with increasing Higgs mass. With a default gluon mass in HERWIG of m_g = 0.75 GeV, it is definitely not within the accuracy of the CMS detector.

Angular distributions can be used to increase signal/background separation in a model dependent analysis (in our case the SM is assumed).

Here some promising angular distributions are presented: $\cos\theta^*_{\vec{P}_{\mu 2-},\vec{P}_{Z1}}$, $\cos\theta^*_{\vec{P}_{\mu 2-},\vec{P}_{Z2}}$, $\cos\Delta\phi = \cos\left[\phi(Z1-plane)-\phi(Z2-plane)\right]$ in the Higgs rest frame, and $\cos\theta_{\vec{P}_{Z1},\vec{P}_{Z2}}$ in the laboratory frame. Muons $\mu 1-$ and $\mu 2-$ are taken from the corresponding Z-bosons. No sensitive differences are observed between LO+PS and NLO.

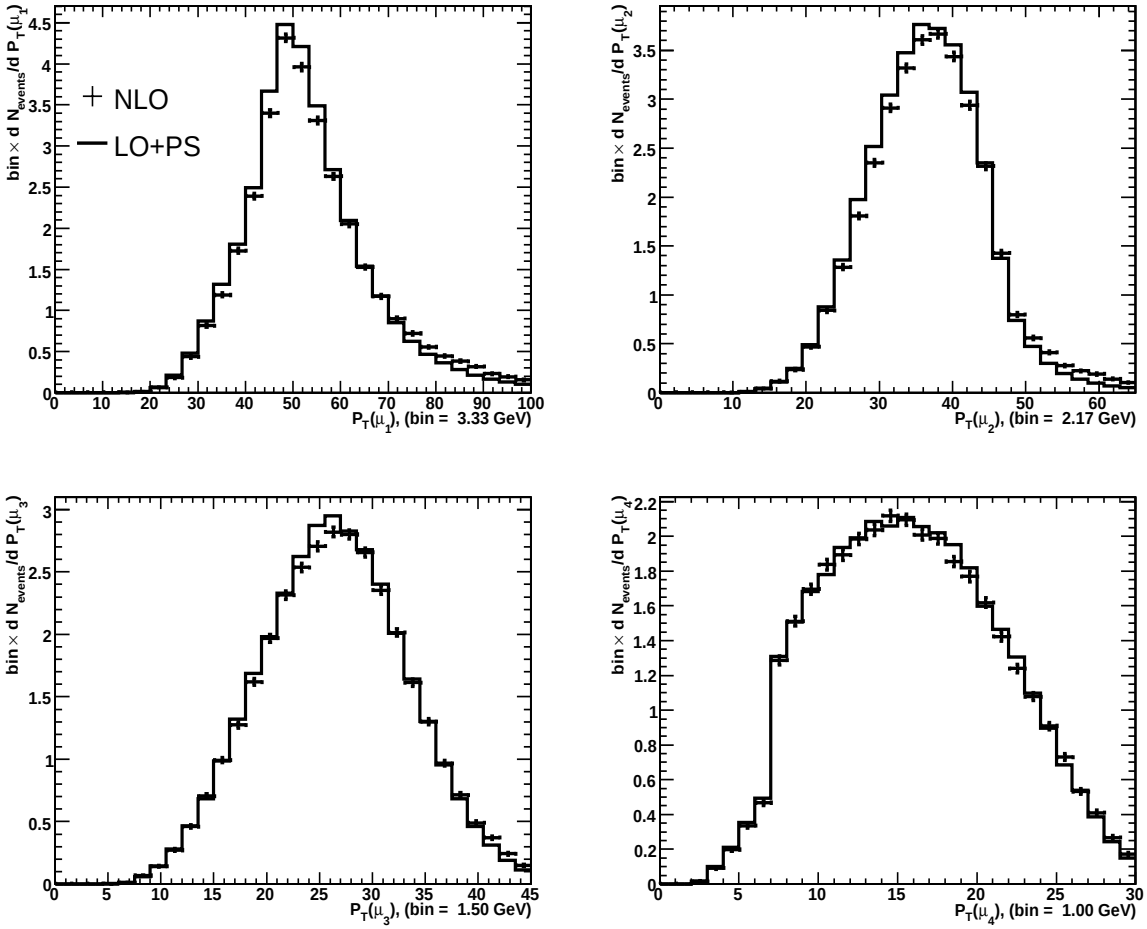

Figure 2: P_T distributions of the four final muons in the Higgs production process (M_H = 150 GeV) at LO+PS and at NLO. The muons are sorted according to their P_T (μ_1 – the highest P_T muon, etc.). The distributions are normalized to 30 fb^{-1} and the selection cuts (see text) are applied. The LO+PS distributions are multiplied by the full NLO/(LO+PS) K-factor for the cuts.

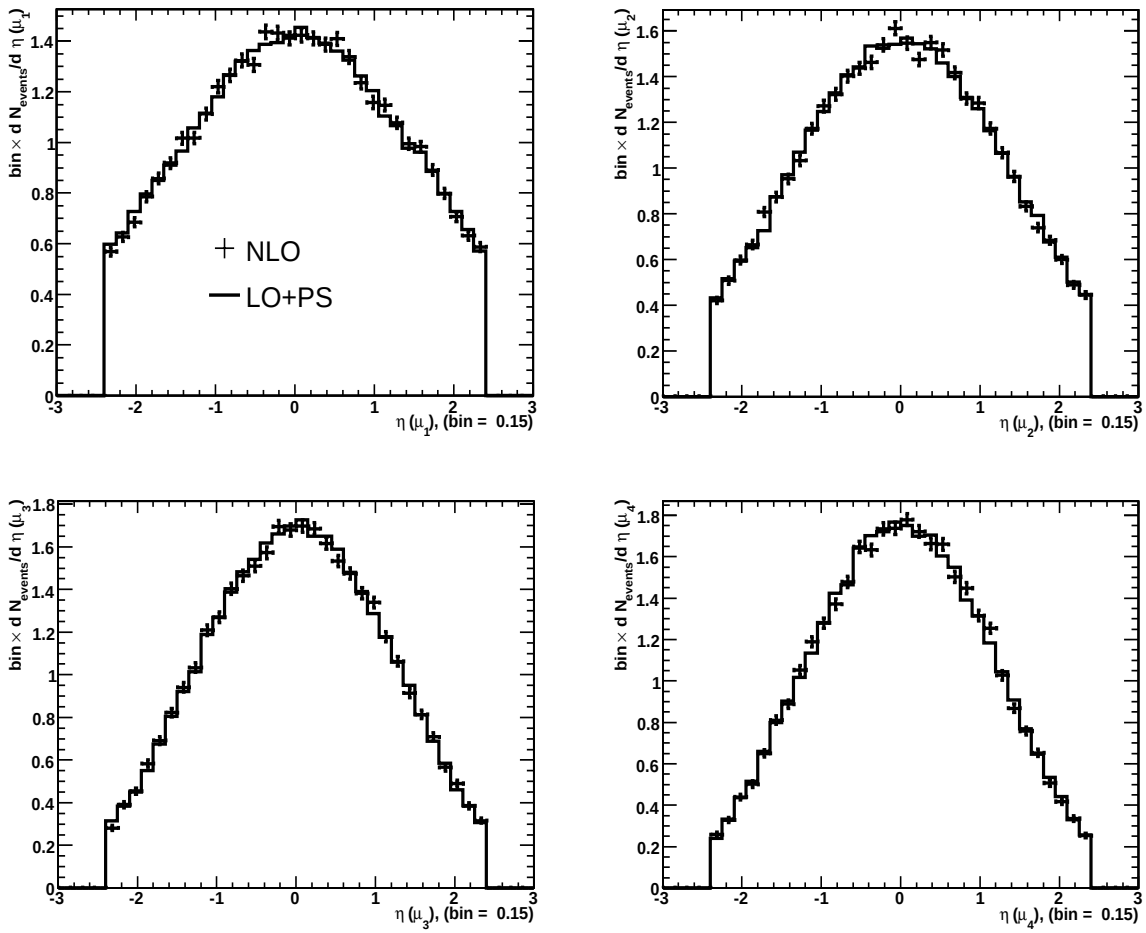

Figure 3: Pseudorapidity distributions of the four final muons in the Higgs production process (M_H = 150 GeV) at LO+PS and at NLO. The muons are sorted according to their P_T (μ_1 – the highest P_T muon, etc.). The distributions are normalized to 30 fb^{-1} and the selection cuts (see text) are applied. The LO+PS distributions are multiplied by the full NLO/(LO+PS) K-factor for the cuts.

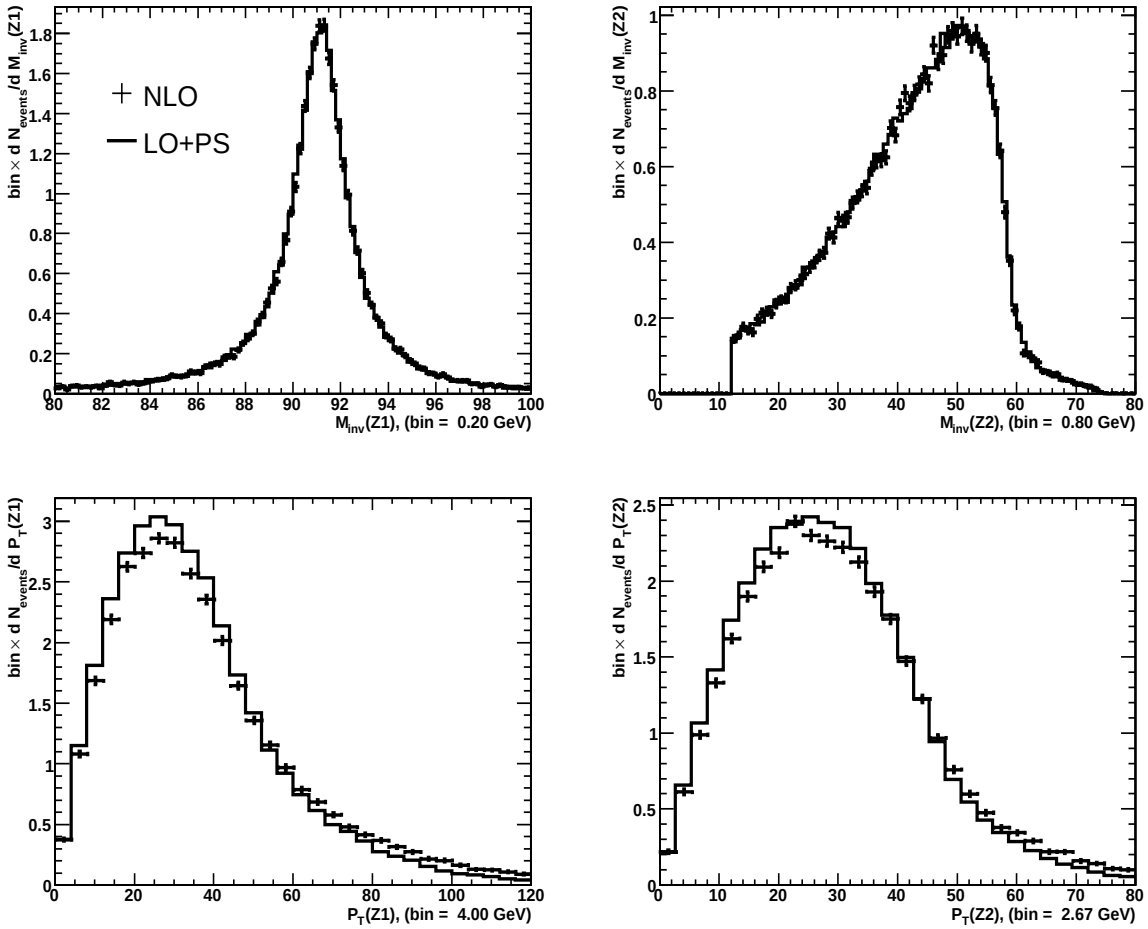

Figure 4: M_{inv} and P_T distributions of the $Z1$- and $Z2$-boson (see the muon combination definitions in the text) in the Higgs production process (M_H = 150 GeV) at LO+PS and at NLO. The distributions are normalized to 30 fb^{-1} and the selection cuts (see text) are applied. The LO+PS distributions are multiplied by the full NLO/(LO+PS) K-factor for the cuts.

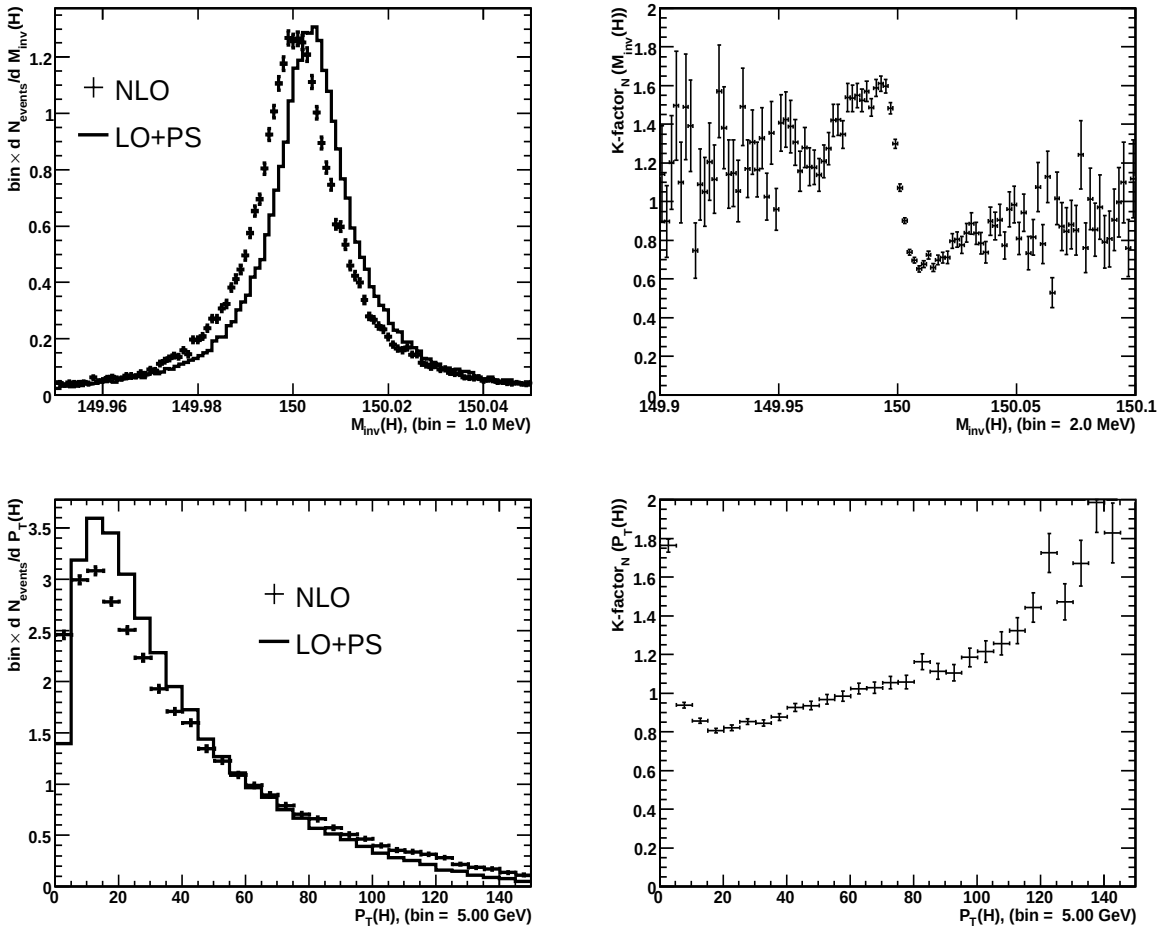

Figure 5: Left plots: M_{inv} and P_T distributions of the Higgs boson in the Higgs production process (M_H = 150 GeV) at LO+PS and at NLO. The distributions are normalized to 30 fb^{-1} and the selection cuts (see text) are applied. The LO+PS distributions are multiplied by the full NLO/(LO+PS) K-factor for the cuts. Right plots: the $M_{inv}(H)$ and $P_T(H)$ dependence of the K-factor (the K-factor is normalized to 1).

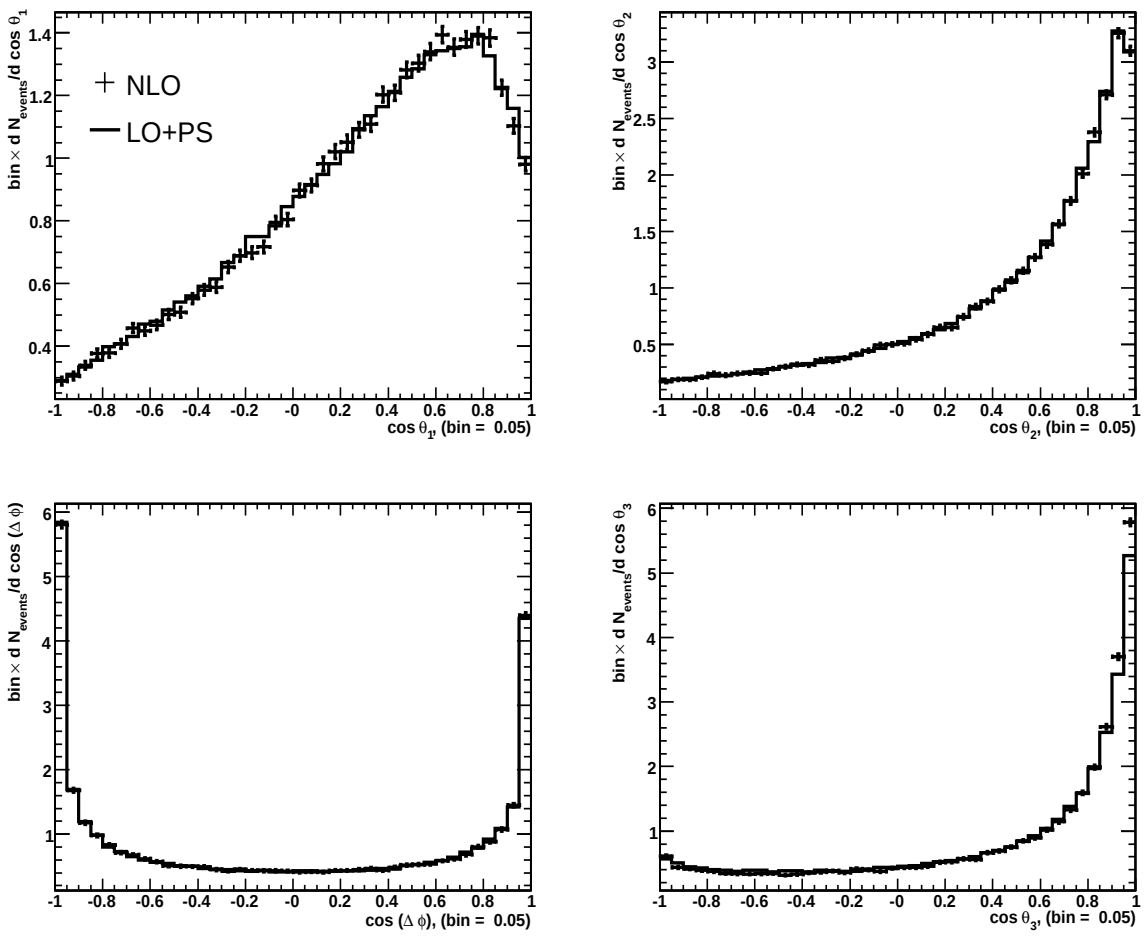

Figure 6: Angular distributions for the Higgs production process (M_H = 150 GeV) at LO+PS and at NLO: $\cos\theta_1 = \cos\theta^*_{\vec{P}_{\mu 2-},\vec{P}_{Z1}}$, $\cos\theta_2 = \cos\theta^*_{\vec{P}_{\mu 2-},\vec{P}_{Z2}}$, $\cos\Delta\phi = \cos\left[\phi(Z1-plane) - \phi(Z2-plane)\right]$. All angles are calculated in the Higgs rest frame. The last angle is $\cos\theta_3 = \cos\theta_{\vec{P}_{Z1},\vec{P}_{Z2}}$ in the laboratory frame. The distributions are normalized to 30 fb^{-1} and the selection cuts (see text) are applied. The LO+PS distributions are multiplied by the full NLO/(LO+PS) K-factor for the cuts.

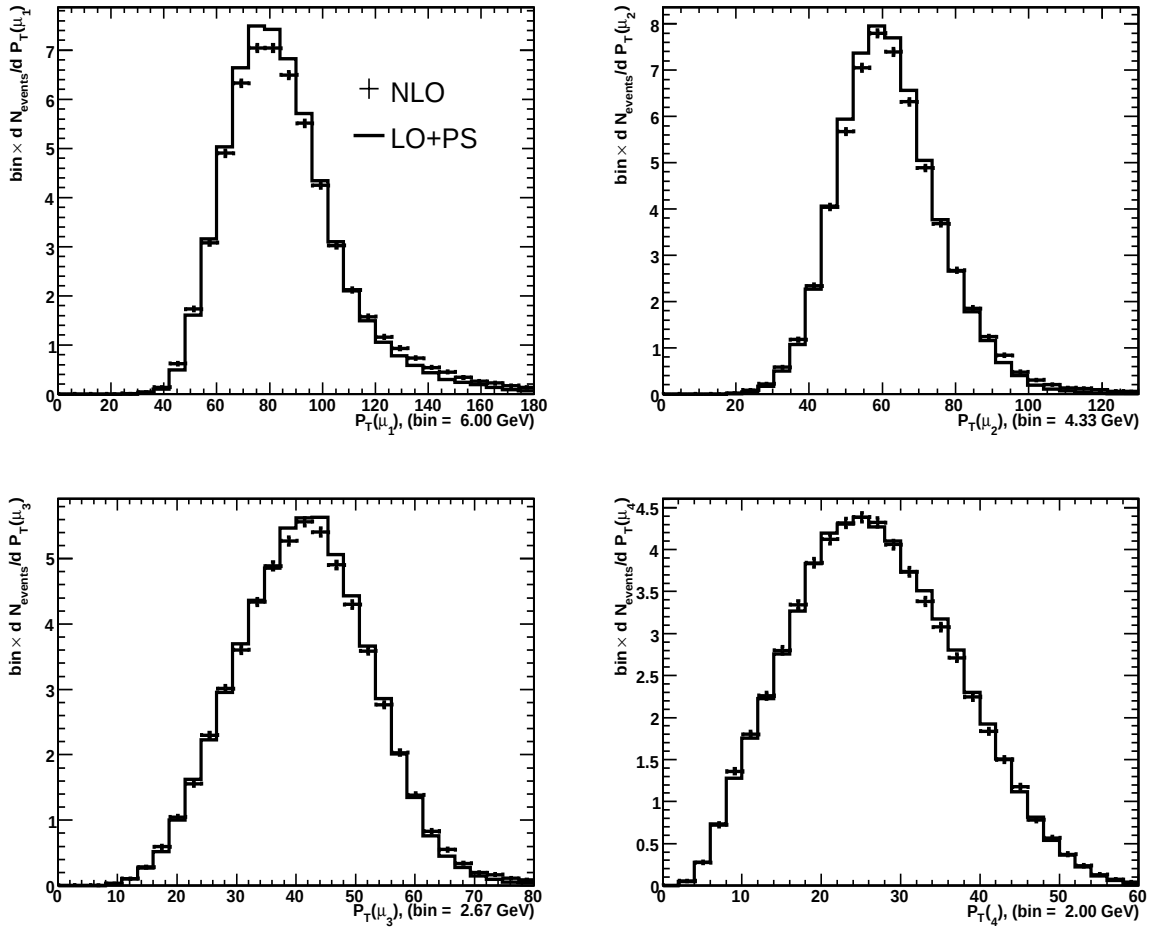

Figure 7: P_T distributions of all four final muons in the Higgs production process (M_H = 250 GeV) at LO+PS and at NLO. The muons are sorted according to their P_T (μ_1 – the highest P_T muon, etc.). The distributions are normalized to 30 fb^{-1} and the selection cuts (see text) are applied. The LO+PS distributions are multiplied by the full NLO/(LO+PS) K-factor for the cuts.

4.2 Monte-Carlo simulation (M_H = 250 GeV)

Kinematical distributions for the Higgs production with M_H = 250 GeV are reported in Figs. 7–11. Qualitative results are very much along the same lines of the ones discussed for the M_H = 150 GeV case.

The P_T and pseudorapidity distributions for all four muons sorted according to their P_T are shown in Figs. 7 and 11. Muons are slightly harder at NLO, especially the highest P_T muon. No large differences between NLO and LO pseudorapidity distributions are observed.

Invariant mass and P_T distributions for the $Z1$- and $Z2$-boson are reported in Fig. 9. The $Z1$-boson is harder at NLO, but the effect is rather small.

Invariant mass and transverse momentum distributions are reported in Fig. 10. The K-factor turns out to increase with P_T, but the effect is smaller than for the M_H = 150 GeV case. The small M_{inv} shift observed at M_H = 150 GeV disappears, but the Higgs peak is broader, as

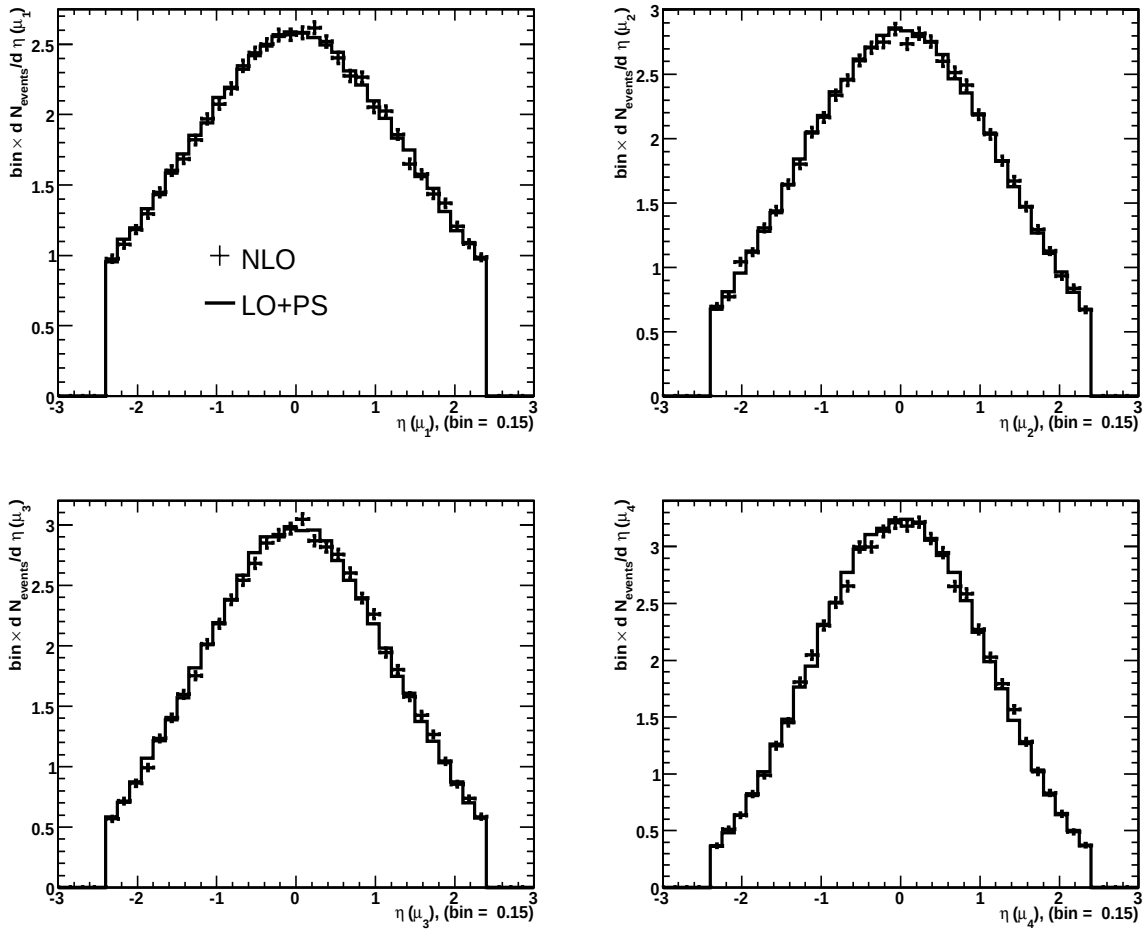

Figure 8: Pseudorapidity distributions of all four final muons in the Higgs production process (M_H = 250 GeV) at LO+PS and at NLO. The muons are sorted according to their P_T (μ_1 – the highest P_T muon, etc.). The distributions are normalized to 30 fb^{-1} and the selection cuts (see text) are applied. The LO+PS distributions are multiplied by the full NLO/(LO+PS) K-factor for the cuts.

expected.

Here we repeat the same angular distributions for the Higgs mass value (250 GeV): $\cos\theta^*_{\vec{P}_{\mu 2-},\vec{P}_{Z1}}$, $\cos\theta^*_{\vec{P}_{\mu 2-},\vec{P}_{Z2}}$, $\cos\left[\phi(Z1-plane)-\phi(Z2-plane)\right]$ in the Higgs rest frame, and $\cos\theta_{\vec{P}_{Z1},\vec{P}_{Z2}}$ in the laboratory frame. Muons $\mu 1-$ and $\mu 2-$ are taken from corresponding Z-bosons. The NLO corrections somewhat change the distribution of the cosine of the angle between momenta of $Z1$- and $Z2$-boson. All other distributions turn out to be identical (up to the precision allowed by Monte Carlo statistics).

5 The $pp \to 2Z/\gamma \to 4\mu$ process

The double Z/γ production is the main irreducible background to the Higgs search at the LHC in the four leptons channel. There are two different types of Feynman diagrams in the process at LO (see Fig. 12). The s-channel diagrams (right plot in Fig. 12) give the main contribution to

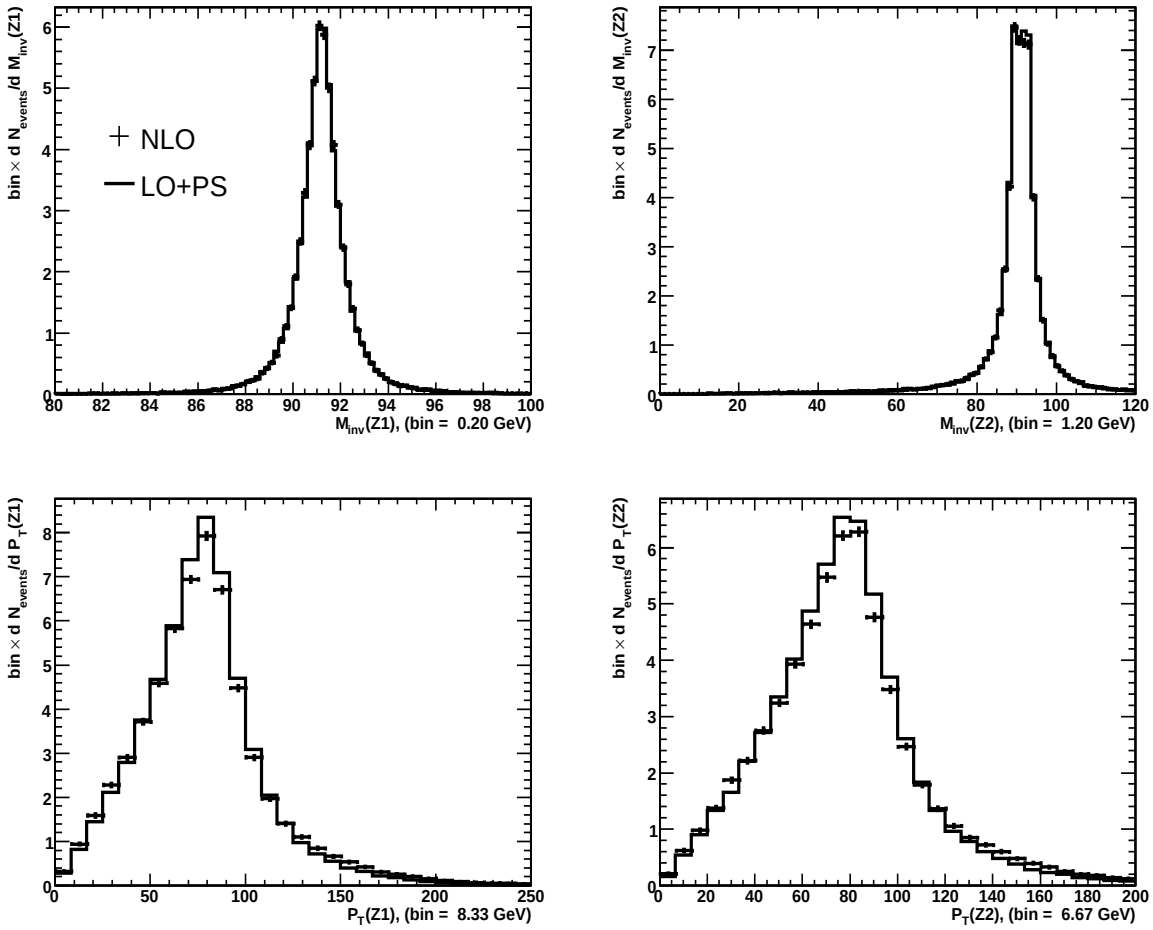

Figure 9: M_{inv} and P_T distributions of the $Z1$- and $Z2$-boson for the Higgs with M_H = 250 GeV (see the particle definitions in the text) at LO+PS and at NLO. The distributions are normalized to 30 fb^{-1} and the selection cuts (see text) are applied. The LO+PS distributions are multiplied by the full NLO/(LO+PS) K-factor for the cuts.

the cross section in the low mass region of $M_{inv}(4\mu)$, in particular below and near M_Z. Since the Higgs mass region below 114.4 GeV has been excluded by LEP data [18], almost all events produced by the s-channel contribution will be removed by selection cuts adopted in a realistic Higgs search analysis (See more details about the problem in [19]). Therefore the t-channel diagrams should be regarded as the relevant effective contributions to the $pp \to 2Z/\gamma \to 4\mu$ process. One of the main impacts of this fact is that one is allowed to use the full cross section at NLO for the considered process taking into account just the t-channel contribution. Certainly, in the whole $M_{inv}(4\mu)$ region the s-channel and the t-channel contributions turn out to have comparable cross sections. NLO diagrams for the process are illustrated in Fig. 13.

5.1 The $pp \to 2Z/\gamma \to 4\mu$ process in an effective NLO approximation

Events at LO can be generated by many tree-level Monte-Carlo programs. We adopted the MadGraph/MadEvent Monte-Carlo generator. The program implements both Z-boson and γ^* contributions, along with their interference, spin correlations of the final muons, and appropriate

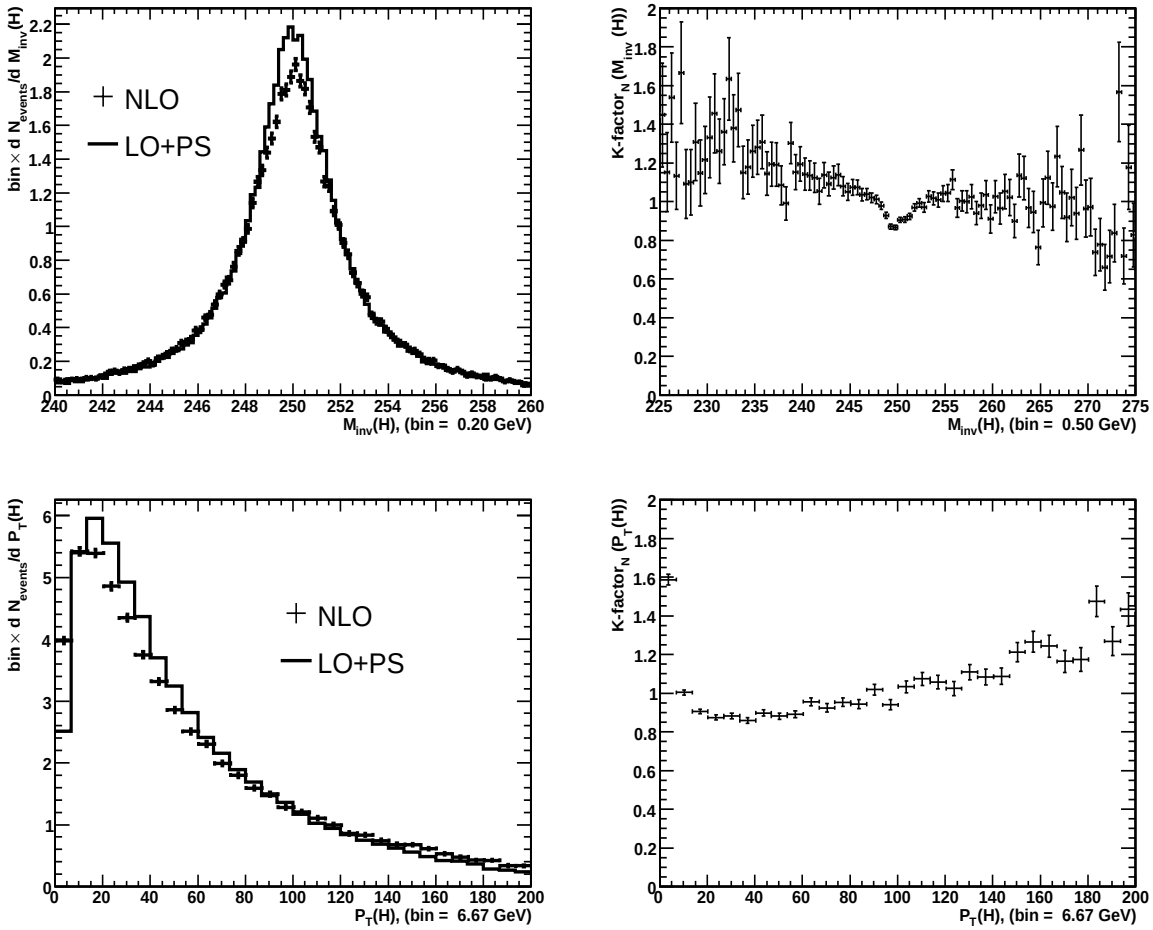

Figure 10: Left plots: M_{inv} and P_T distributions of the Higgs boson in the Higgs production process (M_H = 250 GeV) at LO+PS and at NLO. The distributions are normalized to 30 fb^{-1} and the selection cuts (see text) are applied. The LO+PS distributions are multiplied by the full NLO/(LO+PS) K-factor for the cuts. Right plots: the $M_{inv}(H)$ and $P_T(H)$ dependence of the K-factor (the K-factor is normalized to 1).

Z-boson width.

All the NLO corrections can be sub-divided into two classes: virtual and real corrections. The virtual corrections correspond to the interference between the Feynman LO diagrams and loop diagrams. In the real corrections an extra parton appears in the final state. Some codes can calculate virtual corrections for the double production of real Z-bosons, but they have not included all the effects described above. Events for the real corrections can be generated by tree-level Monte-Carlo codes. However, we can not calculate these corrections separately from virtual ones due to zero mass partons, since infrared poles are absorbed only if these corrections are calculated at the same time. This implies phase space areas where both terms (virtual and real contributions) have unrealistic behavior. One of the methods to address this problem is realized in MC@NLO, where virtual and real corrections are calculated correctly, but without γ contribution and in zero Z-boson width approximation. Unfortunately, this approach is too rough for this study, in particular for the Higgs boson mass smaller than twice the Z-boson mass. That's

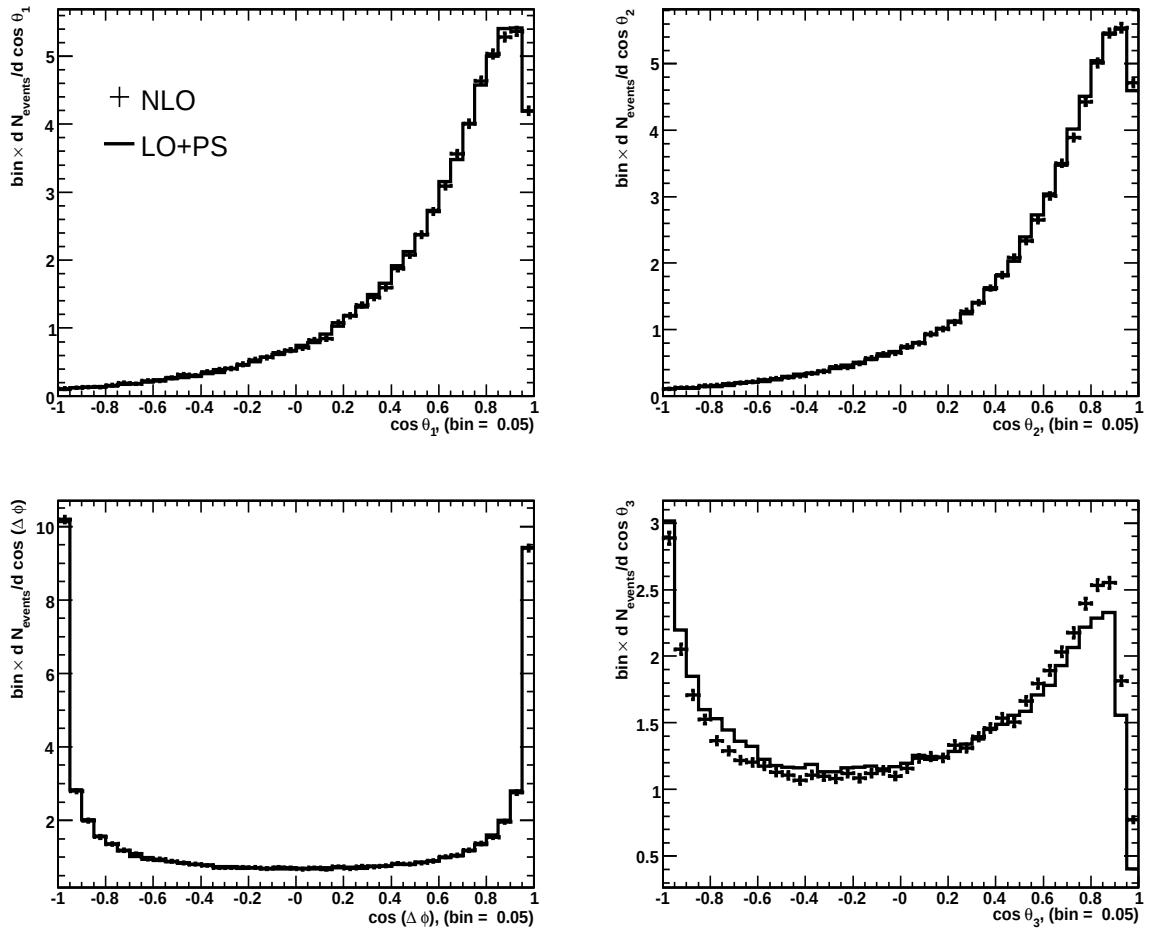

Figure 11: Angular distributions for the Higgs production process (M_H = 250 GeV) at LO+PS and at NLO: $\cos\theta_1 = \cos\theta^*_{\vec{P}_{\mu 2-},\vec{P}_{Z1}}$, $\cos\theta_2 = \cos\theta^*_{\vec{P}_{\mu 2-},\vec{P}_{Z2}}$, $\cos\Delta\phi = \cos\left[\phi(Z1-plane)-\phi(Z2-plane)\right]$. All angles are calculated in the Higgs rest frame. The last angle is $\cos\theta_3 = \cos\theta_{\vec{P}_{Z1},\vec{P}_{Z2}}$ in the laboratory frame. The distributions are normalized to 30 fb^{-1} and the selection cuts (see text) are applied. The LO+PS distributions are multiplied by the full NLO/(LO+PS) K-factor for the cuts.

why we adopt the effective NLO approximation [7].

The general idea of the Effective NLO approximation (hereafter called EffNLO) is the following: the real NLO contribution is calculated with a tree-level Monte-Carlo model in a region where it gives reasonable predictions. In the rest of the phase space the LO approximation is considered, where a showering mechanism is used to simulate the extra parton. After that, samples obtained with the two approaches are mixed up, taking into account their relative cross section. In general one should solve two different problems. First of all, we have to define the limit between the two regions. The second problem is how to mix-up the samples in practice.

In the double Z/γ production we should consider the extra parton radiated by the initial partons only, since there are no QCD partons in the final state at LO. Tree-level calculations for the $pp \to 4\mu + jet$ process clearly give unrealistic results for soft radiation. In order to find the region where the calculation can be applied we can choose the parton P_T as a parameter for

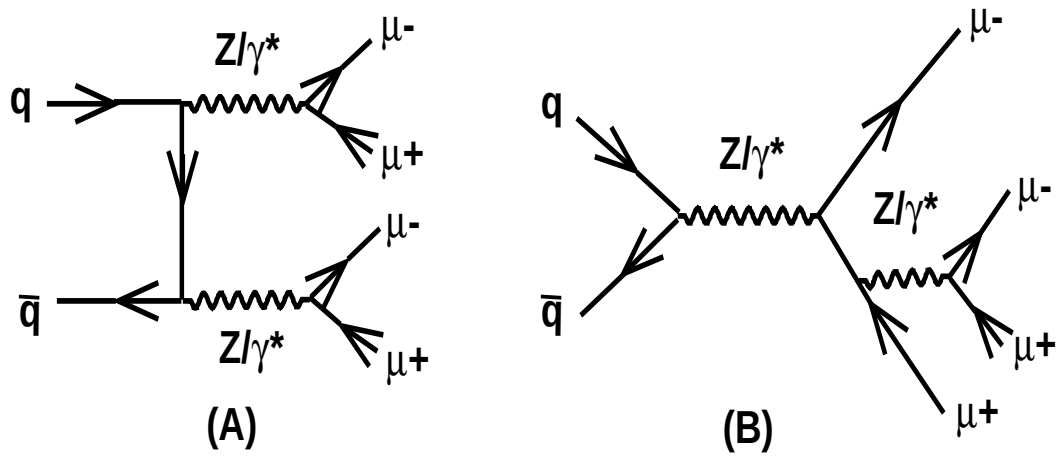

Figure 12: t-channel (A) and s-channel (B) Feynman diagrams at LO for the double Z/γ production with decay to four muons.

the delimitation of the full phase space, by giving a threshold P_T^0. For $P_T(j) > P_T^0$ events, where the extra parton is simulated by a tree-level code, are retained. And with $P_T(j) < P_T^0$ we take events generated by a LO code where the extra parton is generated in the showering mechanism. The most natural condition to fulfill this transition between the two descriptions is the smoothness of the $P_T(j)$ distribution. The only problem which is left is how to include the virtual contribution. We can take into account the events by normalizing the soft region and the natural condition of the normalization is

$$\sigma_{NLO} = K_{norm} \cdot \sigma_{LO}(4\mu)|_{P_T<P_T^0} + \sigma_{LO}(4\mu + j)|_{P_T>P_T^0}$$

This matching scheme gives proper behaviour of the final sample in the high P_T region, where the real corrections describe the shape of the distribution, and reasonable behavior in the low P_T region, where the showering mechanism is appropriate to simulate the events at NLO.

Therefore, the recipe of the EffNLO method is very simple:

- Prepare an event sample at LO with both the Z/γ objects decayed. We produced the sample by MadGraph/MadEvent with the following cuts 5 GeV $< M_{inv}(Z1,\ Z2) <$ 150 GeV, 3 GeV $< P_T(\mu)$, $|\eta(\mu)| <$ 2.4.

- Prepare an event sample of the real NLO correction with both the Z/γ objects decayed. We also produced the sample by MadGraph/MadEvent with the same cuts as above and with an extra cut $P_T(j) >$ 5 GeV.

- Calculate the full cross section (in fact, for the phase space region of the above event samples) at NLO. In our case the cross section was calculated by the MCFM code, taking into account t-channel contribution to the process only.

- Match the samples according to the formula 5.1. In the matching scheme we assume the limit P_T^0 to be stable with respect to all the further applied cuts. We used PYTHIA to simulate the showering partons. Since many partons arise from the initial particles we

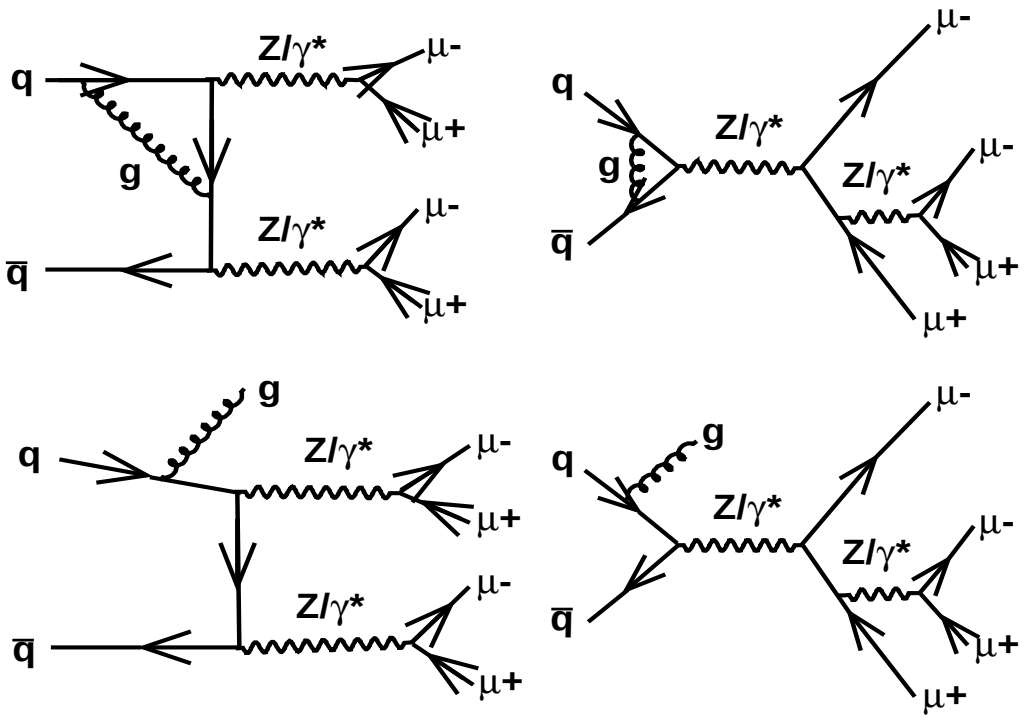

Figure 13: Some representative Feynman diagrams at NLO for the double Z/γ production with decay to four muons.

take the highest P_T parton for the matching. It should correspond to the first branching in the backward showering scheme (in PYTHIA) of the initial state radiation (ISR). In the real NLO correction samples we also switch QCD ISR on, so P_T distribution is smeared slightly near the low edge of the distribution ($P_T(j)$ = 5 GeV).

- FSR QED effects are also taken into account by PYTHIA.

Fig. 14 reports the P_T distribution of the additional parton for both samples and for the final matched NLO event sample, normalized to the corresponding cross sections. As we pointed out the most natural argument to take the proper value of the delimitation parameter P_T^0 is the smoothness of the $P_T(j)$ distribution. We know that in the high P_T region the $pp \to 4\mu + jet$ event sample describes the process properly, so we should go to the low P_T region to find a value of the parameter where the matched distribution looses smoothness. The value is 14 GeV. Also we check values below 14 GeV. If we go to lower P_T values a less part of the 4μ events comes to the NLO sample and a bump appears in the matching point on the NLO distribution. So the smoothness condition is being broken.

5.2 The EffNLO results for the $pp \to 2Z/\gamma \to 4\mu$ process

Kinematical distributions for the double Z/γ-boson production are reported in Figs. 15–19.

P_T and pseudorapidity distributions for all four final muons sorted according to their P_T are shown in Figs. 15 and 16. The highest-P_T, the 2nd-P_T, 3rd-P_T muons are harder in the EffNLO approximation. No big differences are observed for the pseudorapidity distributions.

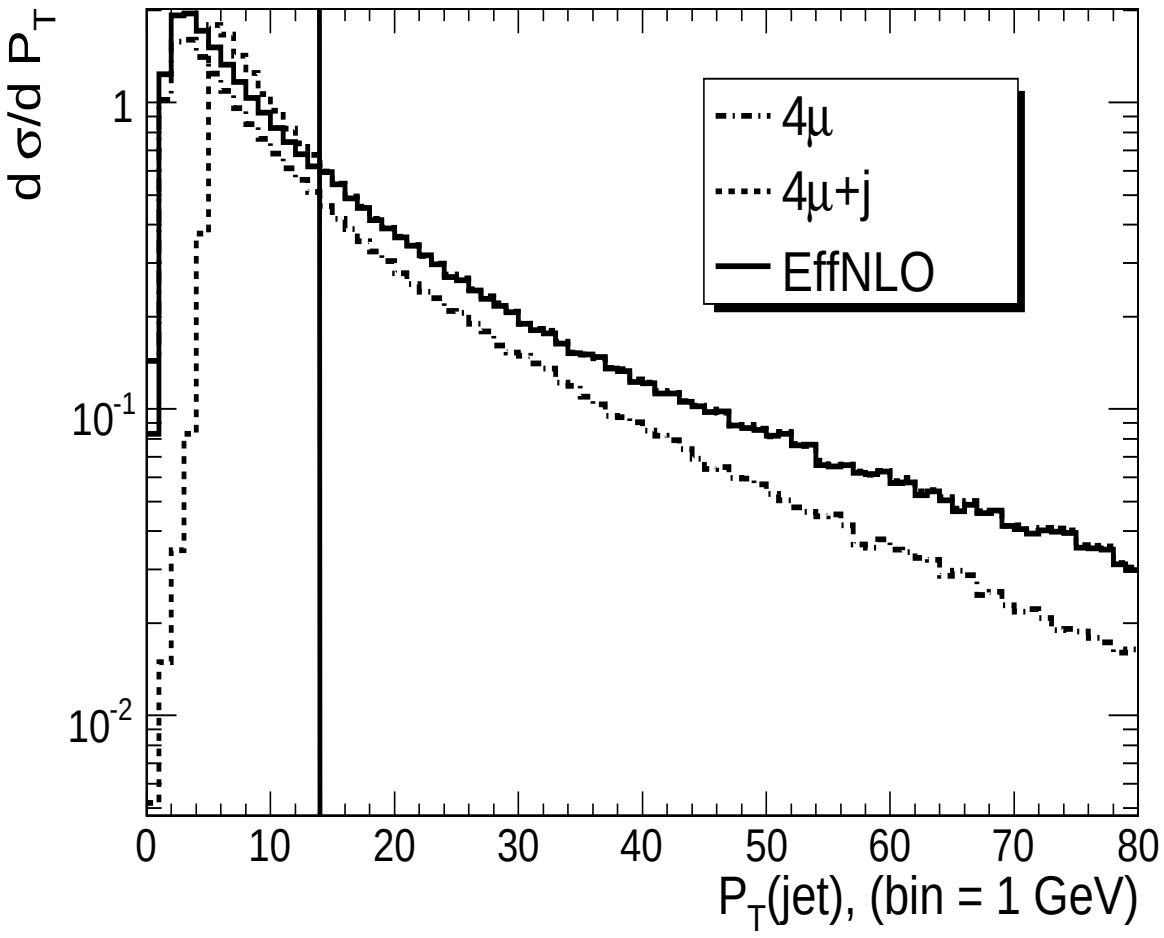

Figure 14: The P_T distribution of the final extra parton for events at LO+PS (dash-dotted line), events of the real NLO correction (dashed line), and events at the Effective NLO approximation (solid line). All distributions are normalized to the corresponding cross sections.

Invariant mass and P_T distributions for the $Z1$- and $Z2$-boson are reported in Fig. 17. Both Z-bosons become harder at EffNLO, but the effect is rather small. Again, the invariant mass distributions do not show any sensitive differences when switching between the two descriptions (EffNLO vs LO).

The mass distribution at LO and at EffNLO is reported in Fig. 18 (top-left). The dependence of the K-factor on the invariant mass is also reported (top-right figure). One can see a sensitive dependency of the K-factor on $M_{inv}(4\mu)$. For lower masses, the EffNLO distribution turns out to be below the LO+PS distribution, but it smoothly increases with $M_{inv}(4\mu)$. We also report the $P_T(4\mu)$ and the K-factor dependence on the observable (a bottom plot in Fig. 18), which turns out to be very sensitive.

For completeness we present the same angular distributions as for the Higgs production events: $\cos\theta^*_{P_{\mu^-},P_{Z1}}$, $\cos\theta^*_{P_{\mu^-},P_{Z2}}$, $\Delta\phi = \phi(Z1-plane) - \phi(Z2-plane)$ in the Higgs rest frame, and $\cos\theta_{P_{Z1},P_{Z2}}$ in the laboratory frame. No large effect on the angular dynamics due to EffNLO corrections is observed.

Table 3: Cross section values for the LO and NLO ZZ samples and the corresponding expected numbers of events for 30 fb^{-1} integrated luminosity. The last column contains K-factors, K=σ_{NLO}/σ_{LO}.

Cuts	LO		NLO		
	σ_{LO}, fb	N_{events}	σ_{NLO}, fb	N_{events}	K-factor
pre-selection cuts	20.1	603	25.5	765	1.27
selection cuts	7.37	221	9.57	287	1.30
$P_T(\mu)$ analysis cuts	6.74	202	8.77	263	1.30
Broad $M_{inv}(4\mu)$ cut	5.77	173	7.57	227	1.31

5.3 The $pp \to 2Z/\gamma \to 4\mu$ process with MCFM

To prepare a NLO approximation we can use NLO codes, which can calculate cross-sections or 1-dimensional distributions only. In this case we should simulate events in the LO+PS approximation and re-wight then according to distributions prepared by the NLO calculator. There is an example of the procedure realized for the Higgs production in [20]. In our case we use MCFM as the NLO code and PYTHIA events [21]. In the note we are interesting in the most important distribution for our analysis – the four muons invariant mass. So overall cross sections and the invariant mass distribution of the four muons for the Standard Model process $pp \to 2Z/\gamma \to 4\mu$ are computed at both LO and NLO with MCFM version 4.0. These simulations are performed within a typical experimental acceptance and for momentum cuts summarized as follows:

- There should be at least four such muons (two opposite sign muon pairs) for an event to be considered.
- $P_T(\mu) > 7$ GeV for all the four muons.
- Selected opposite sign muon pairs arising from Z/γ decays should have an invariant mass $M_{\mu^+\mu^-} > 12$ GeV. This cut on $M_{\mu^+\mu^-}$ removes low-mass off-shell photon contribution.

The calculations with MCFM are carried out for a given fixed set of electroweak input parameters, using the effective field theory approach. The PDF family CTEQ6m1 provided by the CTEQ collaboration [22] is taken as nominal PDF input. The reference cross sections and distributions are obtained with $\mu_R = \mu_F = 2M_Z$. The actual average K-factor in the range 30 GeV $< M_{inv}(4\mu) <$ 750 GeV turns out to be 1.26. However, the average K-factor is re-normalized to the one quoted for $M_{inv}(4\mu) > 100$ GeV, which corresponds to 1.35. The results are summarized in Tab. 4 and presented in Fig. 20. MCFM predicts a smooth increase of the K-factors versus $M_{inv}(4\mu)$, with slightly pronounced local maxima corresponding to $M_{inv}(4\mu) = M_Z$ and $M_{inv}(4\mu) = 2M_Z$. The K-factor can be fitted with a polynomial of 8^{th} order in the range 30 GeV $< M_{inv}(4\mu) <$ 200 GeV, and with an exponential function $a \times (1 - e^{bx})$ in the range 200 GeV $< M_{inv}(4\mu) <$ 750 GeV. The values of the parameters are reported in table 5.

5.4 K-factor: comparison between MCFM and EffNLO approaches

The uncertainties in the K-factor value and $M_{inv}(4\mu)$ dependency for the $pp \to 2Z/\gamma \to 4\mu$ process are estimated from the differences in the MCFM-based results and the EffNLO-based

Table 4: K-factors calculated for different $M_{inv}(4\mu)$ ranges [M_{min} - M_{max}] with MCFM. $K_{MCFM}(M)$ is re-normalized to 1.35 (see text).

M_{min} (GeV)	M_{max} (GeV)	$< M >$ (GeV)	K_{full}	$K_{MCFM}(M) = K_{full}(M) * 1.35/1.26$
113	116	114.5	1.003	1.074
118	121	119.5	1.056	1.132
128	132	130.0	1.097	1.175
138	142	140.0	1.136	1.217
148	152	150.0	1.172	1.256
157	162	159.5	1.199	1.285
167	172	169.5	1.212	1.298
177	182	179.5	1.179	1.263
186	193	189.5	1.170	1.253
195	203	199.0	1.177	1.261
241	257	249.0	1.271	1.362
287	311	299.0	1.339	1.435
329	369	349.0	1.388	1.487
364	428	396.0	1.421	1.522
394	494	444.0	1.448	1.552
417	561	489.0	1.459	1.563
438	650	544.0	1.468	1.573
453	697	575.0	1.473	1.578

Table 5: Results of the fits to the re-normalized K-factors $K_{MCFM}(M_{inv}(4\mu))$ for MCFM. See text for the meaning of the parameters.

p[0]	-4.94682×10^{-1}
p[1]	3.00858×10^{-1}
p[2]	-1.70967×10^{-2}
p[3]	4.51425×10^{-4}
p[4]	-6.46736×10^{-6}
p[5]	5.34046×10^{-8}
p[6]	-2.53992×10^{-10}
p[7]	6.46250×10^{-13}
p[8]	-6.81318×10^{-16}
a	1.595
b	-7.888×10^{-3}

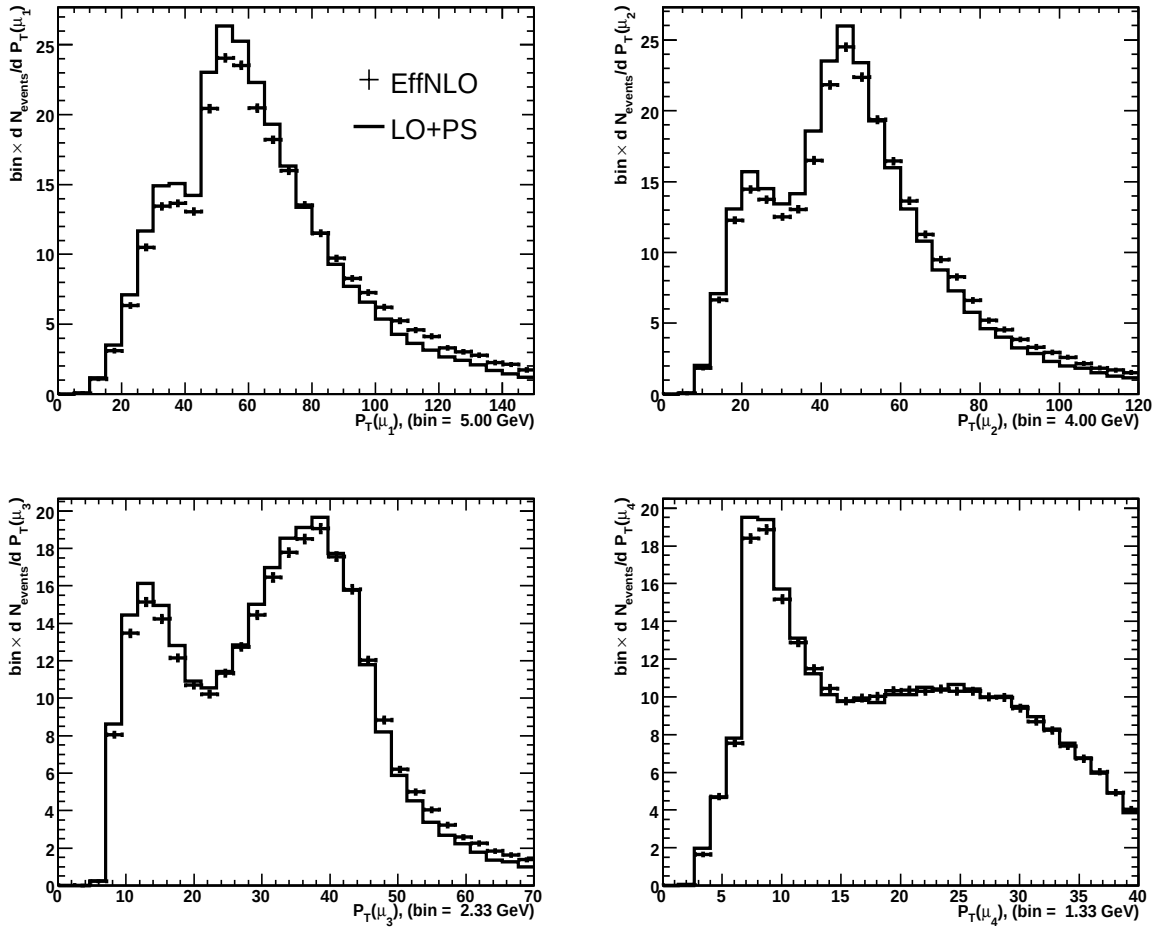

Figure 15: P_T distributions of the four final muons in the double Z/γ-boson production process at LO+PS and in the EffNLO approximation. The muons are sorted according to their P_T (μ_1 corresponds to the muon with the highest P_T, etc.). The distributions are normalized to 30 fb^{-1} and the selection cuts (see text) are applied. The LO+PS distributions are multiplied by the full NLO/(LO+PS) K-factor for the cuts.

results. Fig. 21*a* shows the comparison between the two approaches, restricted to the range where both EffNLO and MCFM calculations are available i.e. for 100 GeV $< M_{inv}(4\mu) <$ 600 GeV. A simple linear combination between 2^{nd} order and 3^{rd} order terms in $(M_{inv}(4\mu) - 250\,GeV)$ turns out to parameterize these differences (Fig. 21*b*) in a convenient way:

$dK/K = a_2(M_{inv}(4\mu) - 250)^2 + a_3(M_{inv}(4\mu) - 250)^3$,
where $a_2 = 2.5 \times 10^{-6}$ and $a_3 = -3.5 \times 10^{-9}$.

6 Implications for the analysis

Tables 6 and 7 summarize the influence of the discussed NLO corrections on the signal and on the double Z/γ background after the application of different experimental selection criteria. In order to facilitate the comparison between the figures at LO and NLO, we multiply the LO numbers by an average K-factor quoted after pre-selection cuts. The tables show that the NLO

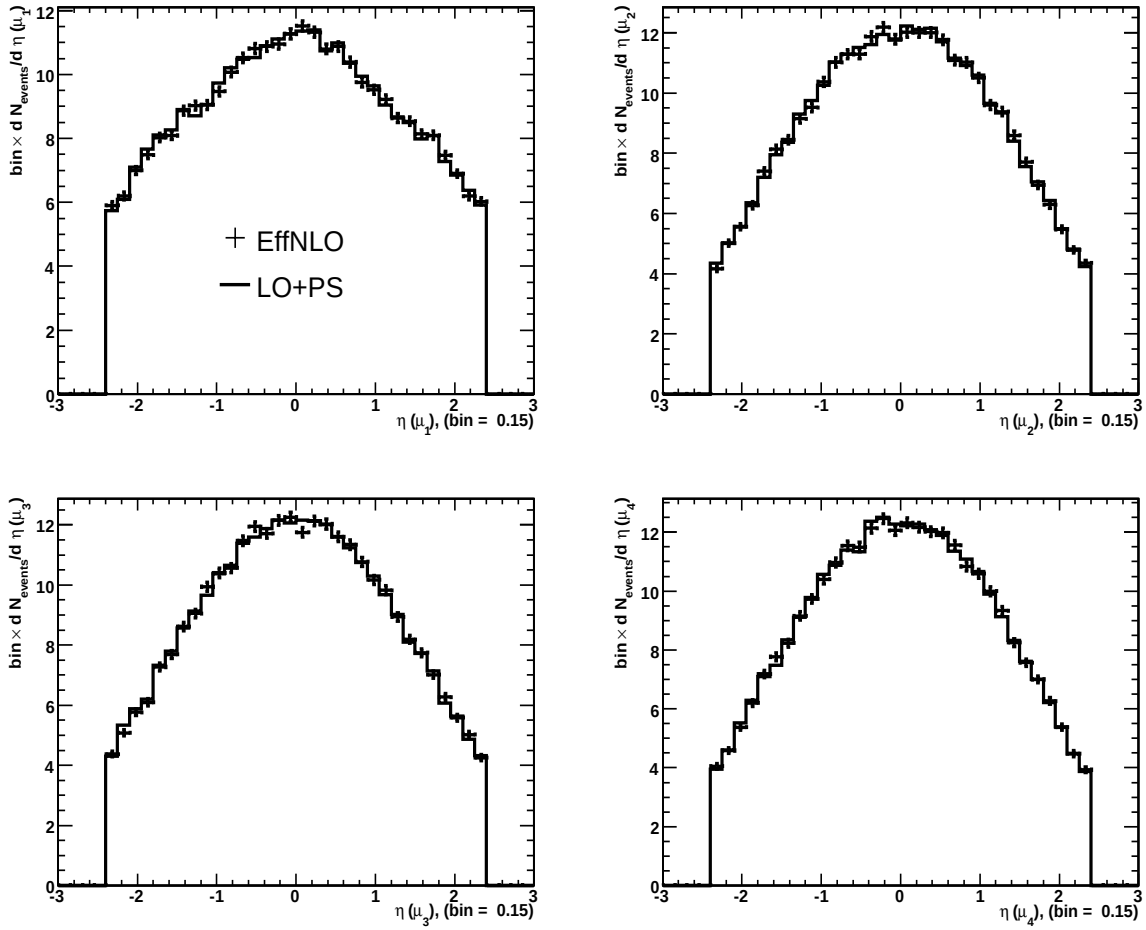

Figure 16: Pseudorapidity distributions of the four final muons in the double Z/γ-boson production process at LO+PS and in the EffNLO approximation. The muons are sorted according to their P_T (μ_1 corresponds to the muon with the highest P_T, etc.). The distributions are normalized to 30 fb^{-1} and the selection cuts (see text) are applied. The LO+PS distributions are multiplied by the full NLO/(LO+PS) K-factor for the cuts.

dynamics is much more important for the background, than for the signal.

The most important aspect of our studies is the K-factor dependence on $M_{inv}(4\mu)$. This observable will play an essential role in signal/background separation, in particular for what concerns the Higgs search in the low mass region, where the Higgs width is extremely small. For example, one can look at the $H \to 4\mu$ analysis at CMS [21]. We should determine the behaviour of this observable with very high accuracy for both signal and backgrounds. Our main conclusion concerning the double Z/γ process is the following. For $M_{inv}(4\mu) < 200$ GeV, the LO prediction tends to overestimate the background. The NLO prediction is above the LO one for $M_{inv}(4\mu) > 200$ GeV.

The NLO dynamics plays an important role on $P_T(4\mu)$. On top of the strong sensitivity on PDF uncertainties [23], this is one of the main arguments to refrain from using the observable in our analysis (where we use the LO event samples).

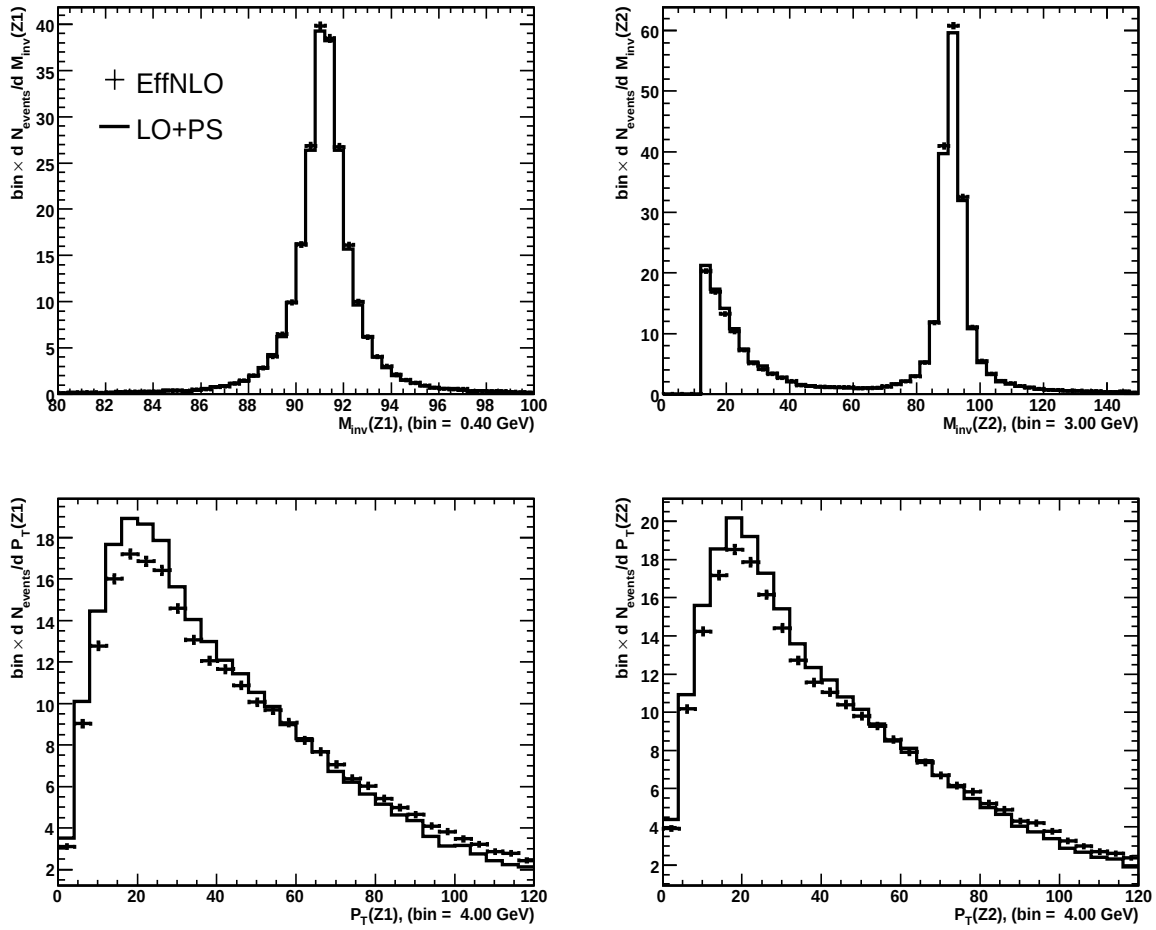

Figure 17: M_{inv} and P_T distributions of the $Z1$- and $Z2$-boson in the double Z/γ-boson production process at LO+PS and in the EffNLO approximation (see the muon combination definitions in the text). The distributions are normalized to 30 fb^{-1} and the selection cuts (see text) are applied. The LO+PS distributions are multiplied by the full NLO/(LO+PS) K-factor for the cuts.

In the note we present two different methods to calculate NLO corrections to the double Z/γ production process simulation, MCFM (exact NLO) and Effective NLO. In fact, they have different areas of application. The former method gives us distributions only, but with exact NLO corrections. In general, one should take this approach when comparing between experimental results and theoretical predictions. However, the adoption of MCFM has clear limitations, which are due to the insufficient description of the final state (missing shower evolution, hadronization etc.). Application of complex selection criteria may not make sense in that context, where it could rather be convenient to adopt EffNLO.

7 Conclusions

NLO corrections to the muon kinematical distributions are analyzed for the signal process $pp \to H \to ZZ^* \to 4\mu$ and for the dominant irreducible background, the double Z/γ production process.

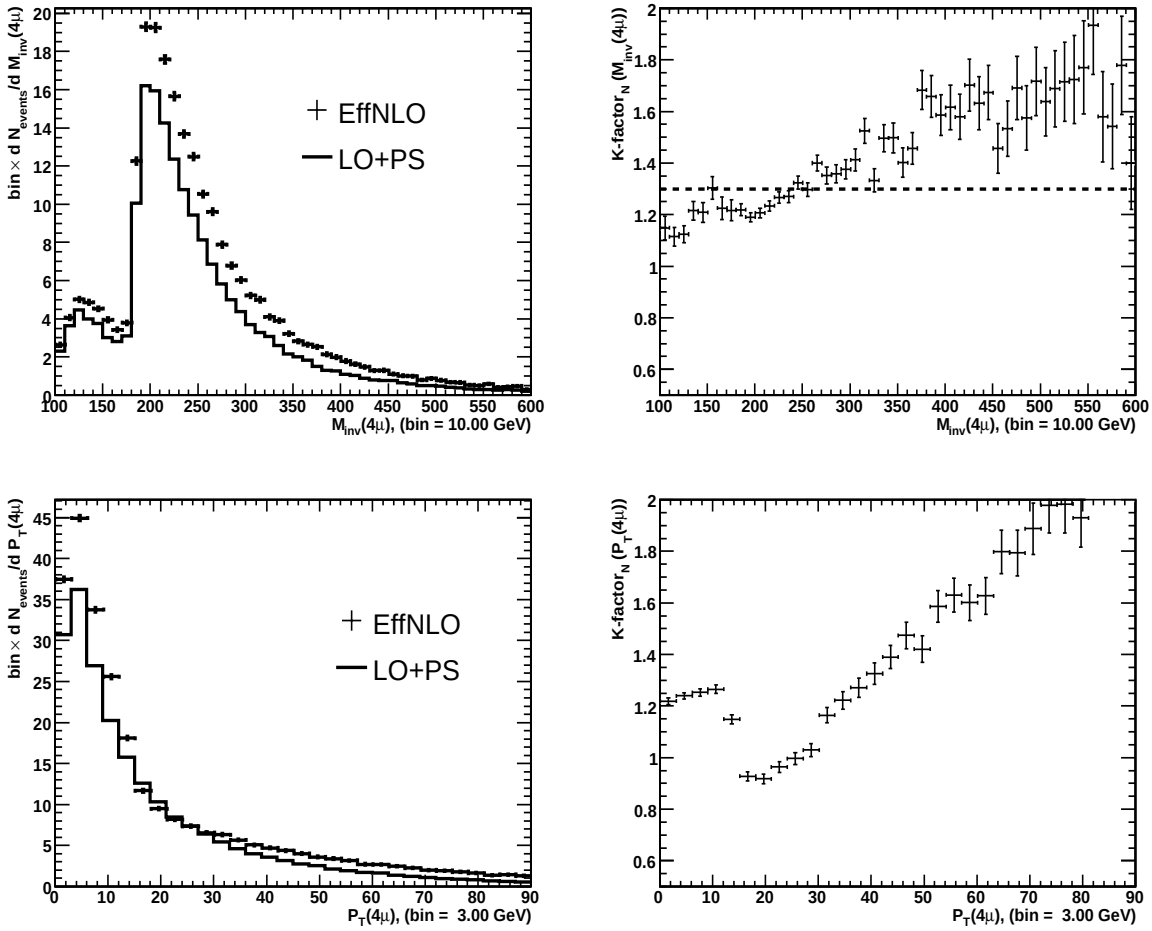

Figure 18: Left plots: M_{inv} and P_T distributions of the 4μ system in the double Z/γ-boson production process at LO+PS and in the EffNLO approximation. The distributions are normalized to 30 fb^{-1} and the selection cuts (see text) are applied. Right plots: the $M_{inv}(H)$ and $P_T(H)$ dependence of the K-factor (the K-factor is normalized to 1).

The impact of NLO dynamics on single muon variables is rather small in both processes. Apart from an overall global correction to the cross sections (the K-factor) the corresponding observables can be used in the analysis without taking into account NLO.

Small shifts in the $M_{inv}(4\mu)$ distribution may influence the mass determination, not the significance in the search, which is rather limited by the experimental resolution. The large effect seen on the $P_T(4\mu)$ distribution does motivate the decision of not using such an observable in order to increase the significance of the signal.

A methodology to take into account the sensitive NLO effects for the double Z/γ production has been proposed, parameterizing the corresponding K-factors (and the relative uncertainty) in terms of $M_{inv}(4\mu)$.

New improvements are possible in simulation of the considered processes. The main necessary improvements in the double Z/γ process calculation are inclusion of the s-channel contribution and muon permutations in the full NLO calculation. An improved version of the MC@NLO ap-

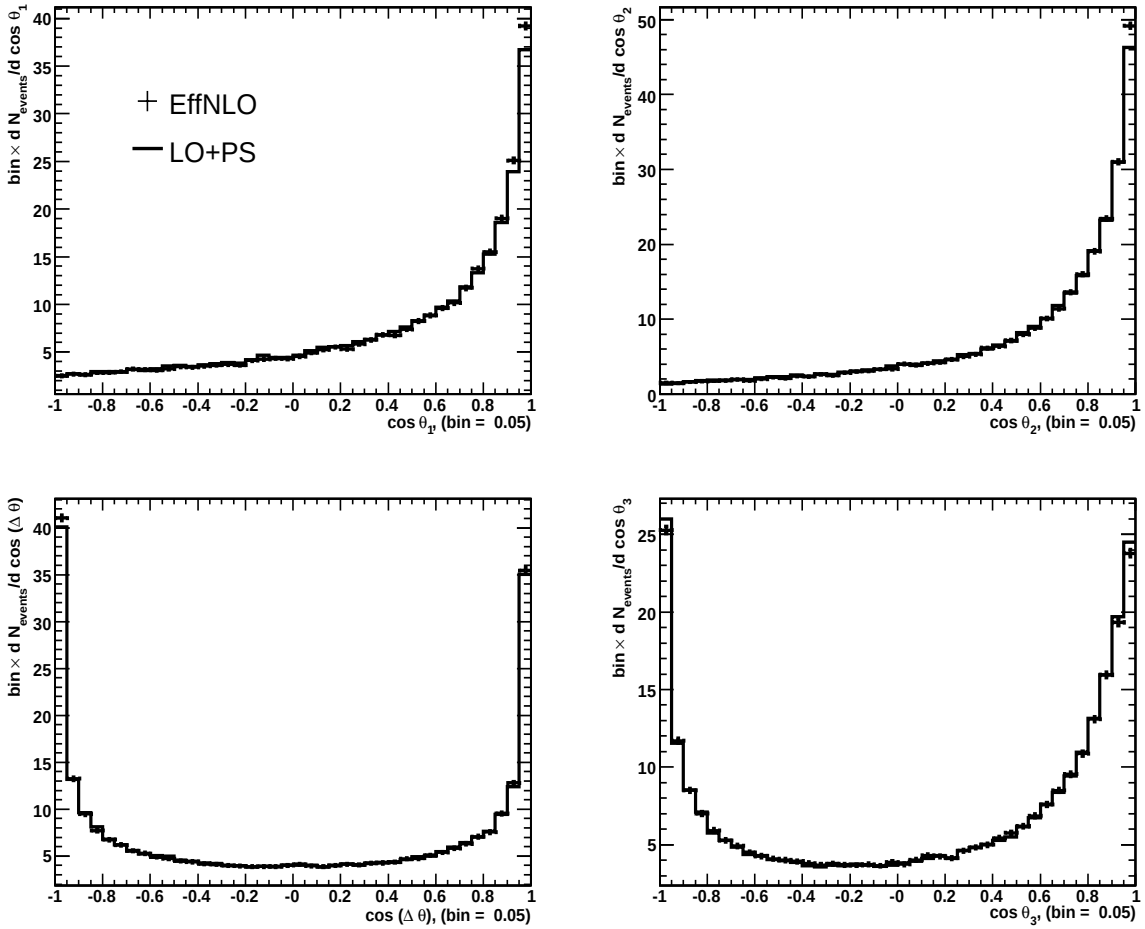

Figure 19: Angular distributions for the double Z/γ-boson production process at LO+PS and in the EffNLO approximation: $\cos\theta_1 = \cos\theta^*_{\vec{P}_{\mu 2-},\vec{P}_{Z1}}$, $\cos\theta_2 = \cos\theta^*_{\vec{P}_{\mu 2-},\vec{P}_{Z2}}$, $\cos\Delta\phi = \cos\left[\phi(Z1-plane)-\phi(Z2-plane)\right]$. All angles are calculated in the Higgs rest frame. The last angle is $\cos\theta_3 = \cos\theta_{\vec{P}_{Z1},\vec{P}_{Z2}}$ in the laboratory frame. The distributions are normalized to 30 fb^{-1} and the selection cuts (see text) are applied. The LO+PS distributions are multiplied by the full NLO/(LO+PS) K-factor for the cuts.

proach with taking into account Z-boson width, s-channel contribution, and muon permutations, could be adapted for the process. If experiments will require NNLO accuracy for the processes, especially for the Higgs production simulation, re-weighting procedures could be used. One of them is proposed in [24].

8 Acknowledgements

We would like to thank A. Ballestrero and G. Dissertori for their useful remarks and comments on the text of the Note. A.Sh. would like to acknowledge support from the RFBI grant 04-02-17448 and the Russian Ministry of Education and Science grant NS.8122.2006.2.

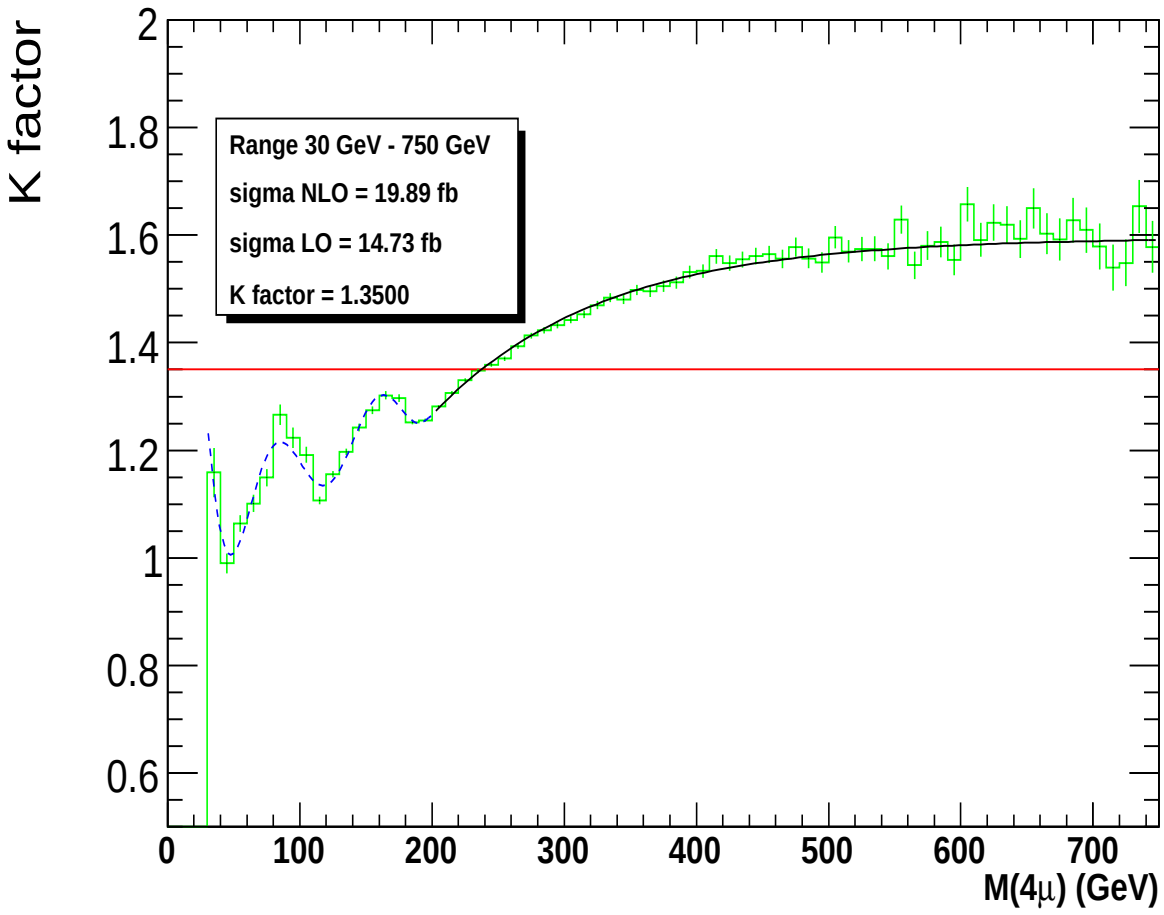

Figure 20: MCFM: Dependence of the re-normalized K-factor on $M_{inv}(4\mu)$. Selection cuts as described in the text are applied. A polynomial fit in the region 30 GeV $< M_{inv}(4\mu) <$ 200 GeV (dashed blue line), an exponential fit in the region 200 GeV $< M_{inv}(4\mu) <$ 750 GeV (solid black line) and the average K-factor for $M_{inv}(4\mu) >$ 100 GeV (solid red line) are superimposed (see text for the results of the fits).

References

[1] A. Djouadi, arXiv:hep-ph/0503172.

[2] S. Abdullin *et al.*, Eur. Phys. J. C **39S2** (2005) 41.

[3] J. Tanaka, Nucl. Phys. Proc. Suppl. **144** (2005) 341.

[4] M. Spira, A. Djouadi, D. Graudenz and P. M. Zerwas, Nucl. Phys. B **453** (1995) 17 [arXiv:hep-ph/9504378].

[5] S. Frixione and B. R. Webber, JHEP **0206**, 029 (2002) [arXiv:hep-ph/0204244].

[6] L. J. Dixon, Z. Kunszt and A. Signer, Phys. Rev. D **60** (1999) 114037 [arXiv:hep-ph/9907305].

[7] E. Boos et al. CMS NOTE-2000/065.

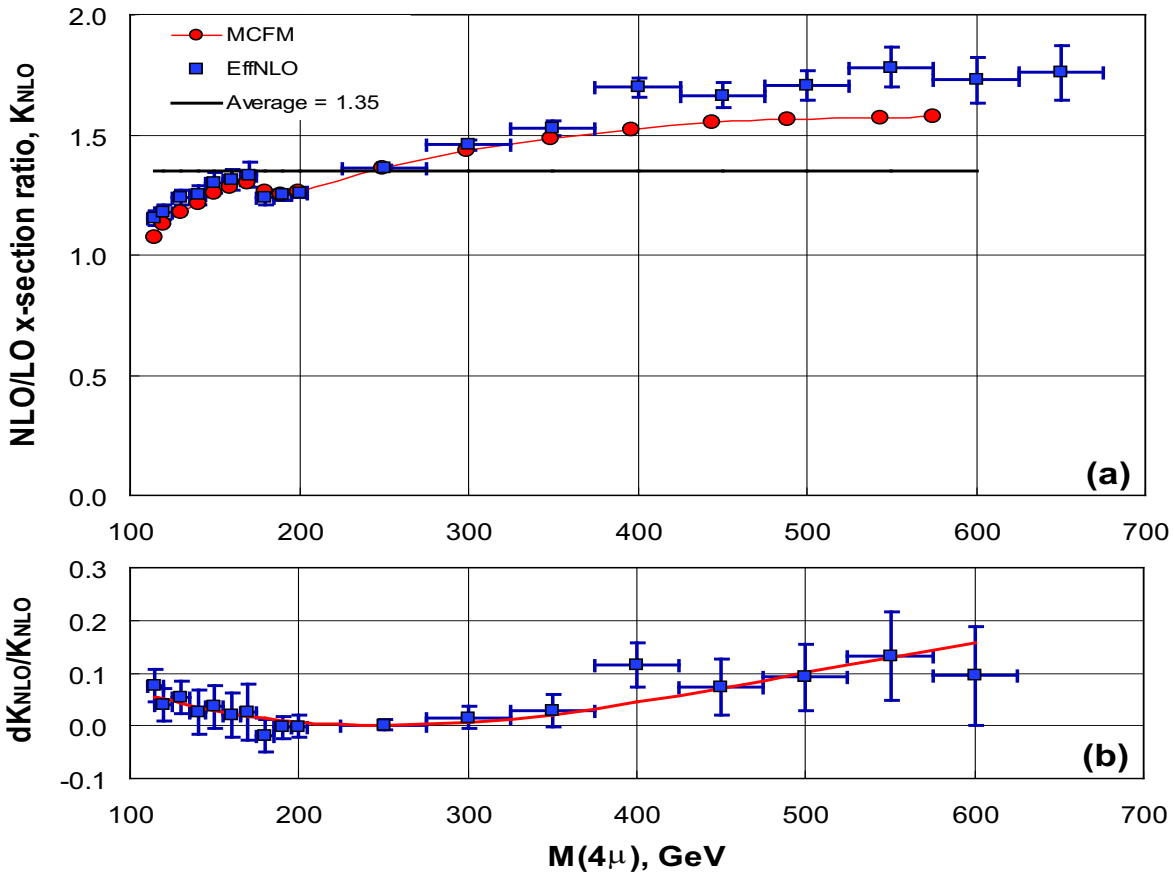

Figure 21: (*a*) K-factor versus $M_{inv}(4\mu)$ predicted by MCFM (red circles) and EffNLO (blue squares). (*b*) Differences between the predictions of EffNLO and MCFM for the K-factor versus $M_{inv}(4\mu)$. A parameterization of the difference (red solid line) is described in the text.

[8] G. Corcella *et al.*, JHEP **0101**, 010 (2001) [arXiv:hep-ph/0011363].
Official site: http://hepwww.rl.ac.uk/theory/seymour/herwig

[9] F. Maltoni and T. Stelzer, JHEP **0302**, 027 (2003) [arXiv:hep-ph/0208156].
Official site: http://madgraph.hep.uiuc.edu

[10] S. Frixione and B. R. Webber, arXiv:hep-ph/0506182.
Official site: http://www.hep.phy.cam.ac.uk/theory/webber/MCatNLO

[11] T. Sjostrand, P. Eden, C. Friberg, L. Lonnblad, G. Miu, S. Mrenna and E. Norrbin, Comput. Phys. Commun. **135** (2001) 238 [arXiv:hep-ph/0010017].
Official site: http://www.thep.lu.se/ torbjorn/Pythia.html

[12] J. M. Campbell and R. K. Ellis, Phys. Rev. D **60**, 113006 (1999) [arXiv:hep-ph/9905386].
Official site: http://mcfm.fnal.gov

[13] A. Djouadi, J. Kalinowski and M. Spira, Comput. Phys. Commun. **108**, 56 (1998) [arXiv:hep-ph/9704448]. Official site: http://people.web.psi.ch/spira/proglist.html

Table 6: Number of signal and background events for $M_H = 150$ GeV and L=30 $fb^{-}1$. The LO numbers are multiplied by an average K-factor quoted after pre-selection cuts.

	Signal K * LO	Signal NLO	ZZ Background K * LO	ZZ Background NLO
Pre-selection cuts	39.3	39.3	603	765
Selection cuts	34.7	34.8	280	287
$P_T(\mu)$ analysis cuts	32.9	33.0	256	263
Broad $M_{inv}(4\mu)$ cut	32.9	33.0	219	227

Table 7: Number of signal events and background events for $M_H = 250$ GeV for L=30 $fb^{-}1$.

	Signal LO * K	Signal NLO	ZZ Background LO * K	ZZ Background NLO
Pre-selection cuts	60.9	60.9	603	765
Selection cuts	59.9	59.9	221	287
Analysis cuts	59.1	59.1	202	263
Broad $M_{inv}(4\mu)$ cut	59.1	59.1	219	227

[14] H. Murayama, I. Watanabe and K. Hagiwara, KEK-91-11

[15] H. L. Lai *et al.* [CTEQ Collaboration], Eur. Phys. J. C **12** (2000) 375 [arXiv:hep-ph/9903282].

[16] M. Spira, Fortsch. Phys. **46** (1998) 203 [arXiv:hep-ph/9705337].

[17] M. Seymour, private communictions.

[18] R. Barate *et al.* [LEP Working Group for Higgs boson searches], Phys. Lett. B **565** (2003) 61 [arXiv:hep-ex/0306033].

[19] S. Abdullin et al., "Relative contributions of t- and s-channels to the $pp \to 2Z/\gamma \to 4\mu$ process", CMS NOTE-2006/057.

[20] G. Davatz, G. Dissertori, M. Dittmar, M. Grazzini and F. Pauss, JHEP **0405** (2004) 009 [arXiv:hep-ph/0402218].

[21] S. Abdullin et al., "Search for $pp \to H \to 4\mu$ using $M(4\mu)$-dependent cuts", CMS NOTE-2006/122.

[22] D. Stump, J. Huston, J. Pumplin, W. K. Tung, H. L. Lai, S. Kuhlmann and J. F. Owens, JHEP **0310**, 046 (2003) [arXiv:hep-ph/0303013].

[23] S. Abdullin et al., "Study of PDF and QCD scale uncertainties in $pp \to 2Z/\gamma \to 4\mu$ events at the LHC", CMS NOTE-2006/068.

[24] G. Davatz, F. Stockli, C. Anastasiou, G. Dissertori, M. Dittmar, K. Melnikov and F. Petriello, arXiv:hep-ph/0604077.